Master thesis

A study of quasi ballistic conduction in advanced MOSFET using RT model

Supervisor

Professor Hiroshi Iwai

Iwai Laboratory

Department of Advanced Applied Electronics

Tokyo Institute of Technology

06M36516

Yasuhiro Morozumi

Contents

Chapter 1

Introduction

1.1The present situation in LSI

Our circumstance is filled with various electronic manufactures such as a mobile telephone, a game console and PC. The evolution of the performance of those products surprises us. The core of evolution of the performance is progress of the LSI technology. The progress of the LSI technology improved calculation ability of their electronic manufactures drastically. For example, figure 1.1 shows Moore's Law said to become double the accumulation density of the semiconductor in 18-24 months. The quantity of the transistors has increased exponentially and the quantity will increase continuously from now on. [1.1] Many of LSI consist of MOSFET（metal oxide semiconductor field effect transistor） of a basic element device. MOSFET has evolved by its scaling with evolution of LSI. The MOSFET is a transistor consisting of the gate electrode, the source electrode, the drain electrode, the gate insulator film and a substrate like figure 1.2. [1.2] The gate length which expresses the distance from the source to the drain is shorter than 35[nm] in 2005 years. [1.3] The gate length will be short by progress scaling from now on.

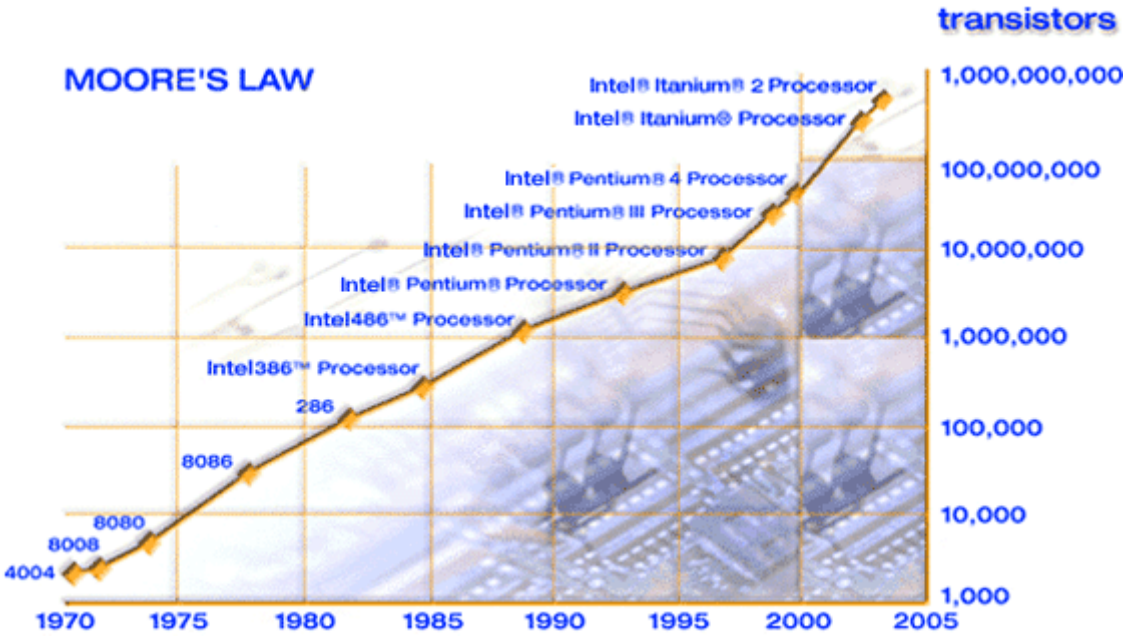

Figure 1.1 Moore's law

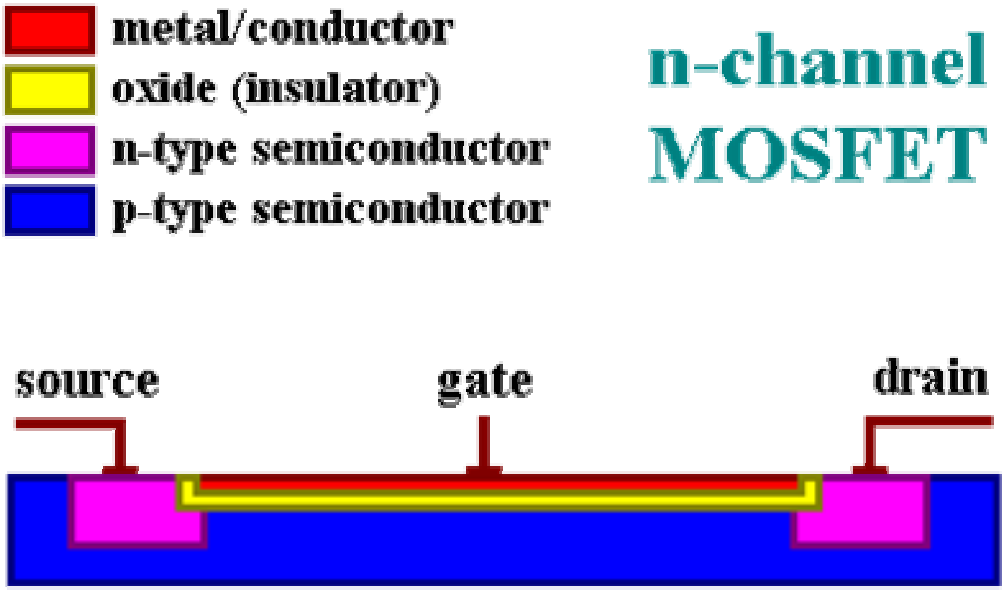

Figure 1.2 the structure of MOSFET

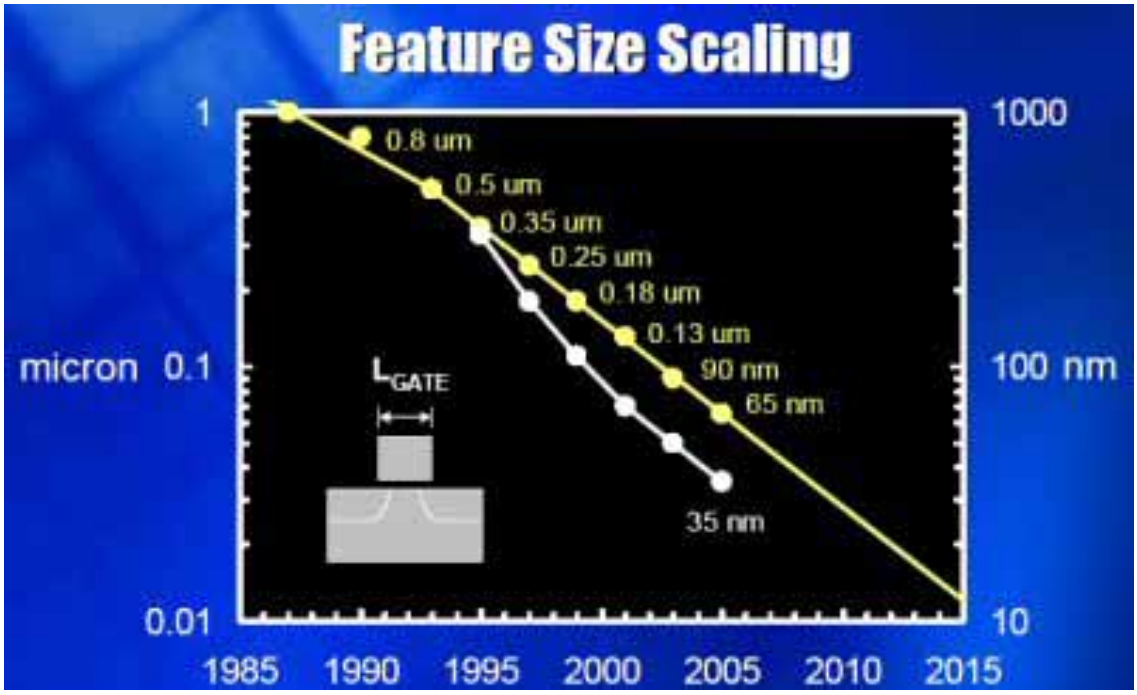

Figure 1.3 the scaled gate length

1.2 The short gate length and the ballistic conductivity

MOSFET changes "on state" which can carry the drain current when the gate bias exceeds the threshold voltage. Then the drain bias make the electron move from the source to drain with the drain current in on state of MOSFET. The electrons flow is observed as the drain current in macroscopic but each electrons move the various way like figure 1.4. Each electron has the scattering probability by mainly three scattering factors in MOSFET. Its factor is the impurity by doping, roughness of between gate insulator film and the silicon, and phonon of the atomic oscillation. Like this, various behaving electrons move statically from the source to the drain. But in the advanced scaling MOSFET, the way which each electron moves to the drain becomes important in no statistical thought because no scattering electrons increase by shorter scaled gate length like figure 1.5. The drain current increases by these electrons. This phenomenon

is called as the ballistic conductivity in MOSFET. When perfect ballistic current is defined as 1, its actual current ratio as against 1 is called as ballisticity. To increase ballisticity will become the problem in scaled MOSFET from now on.

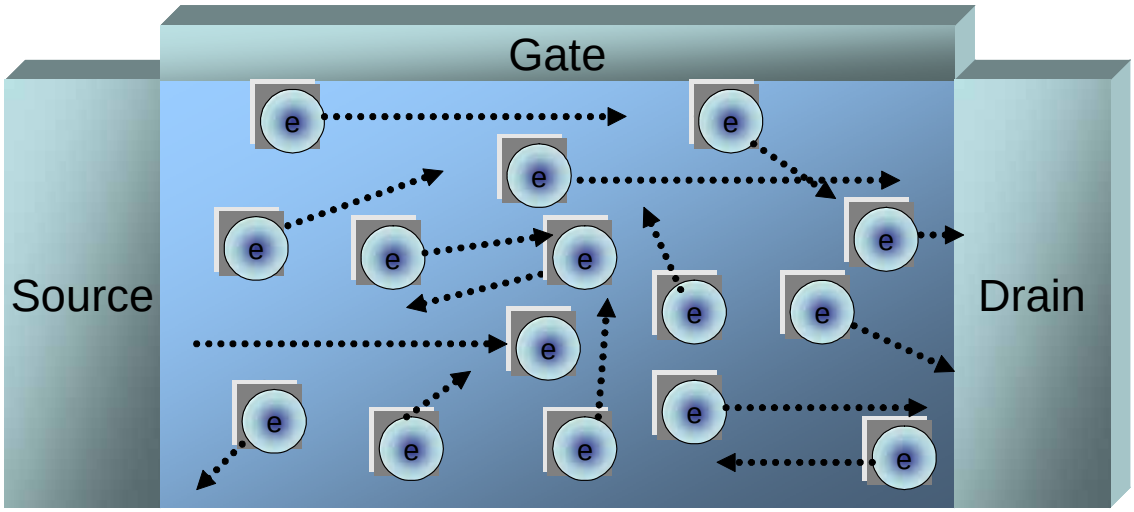

Figure 1.4 various electrons flux

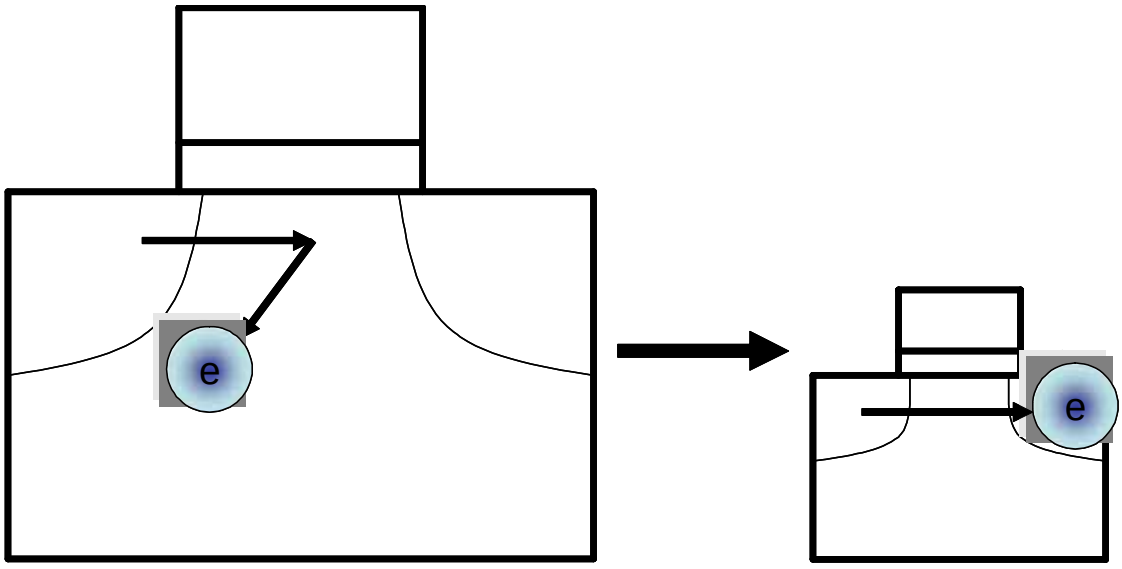

Figure 1.5 ballistic conduction occurring by scaling

1.3 ITRS and ballistic conductivity

ITRS makes the index that how much ratio this ballistic conduction is regarded as important. [1.4]

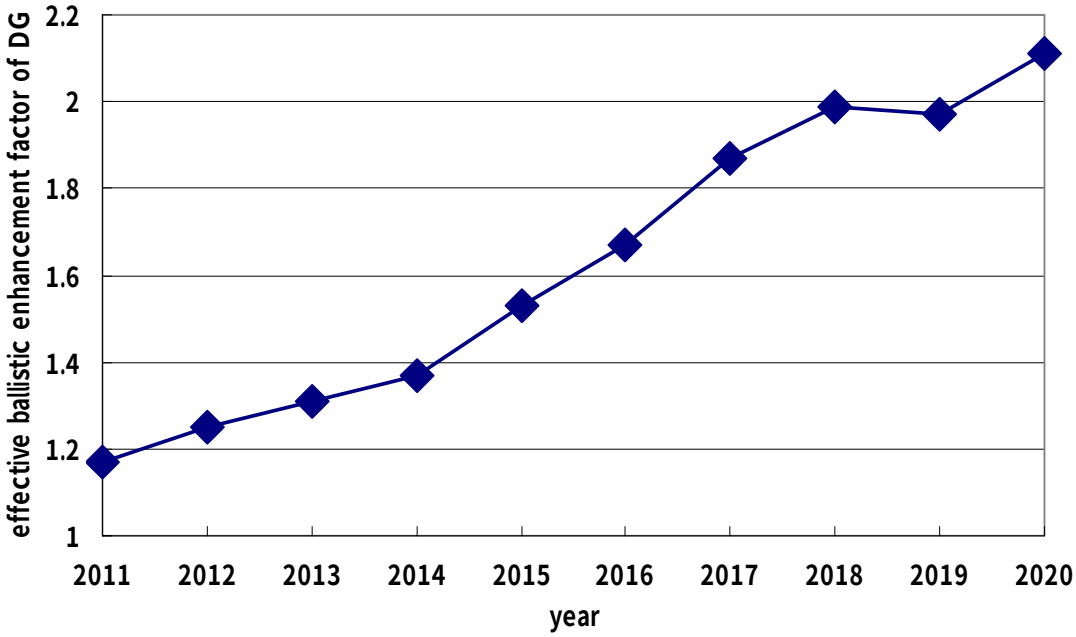

Figure 1.6 the prediction of the effect of ballistic conduction

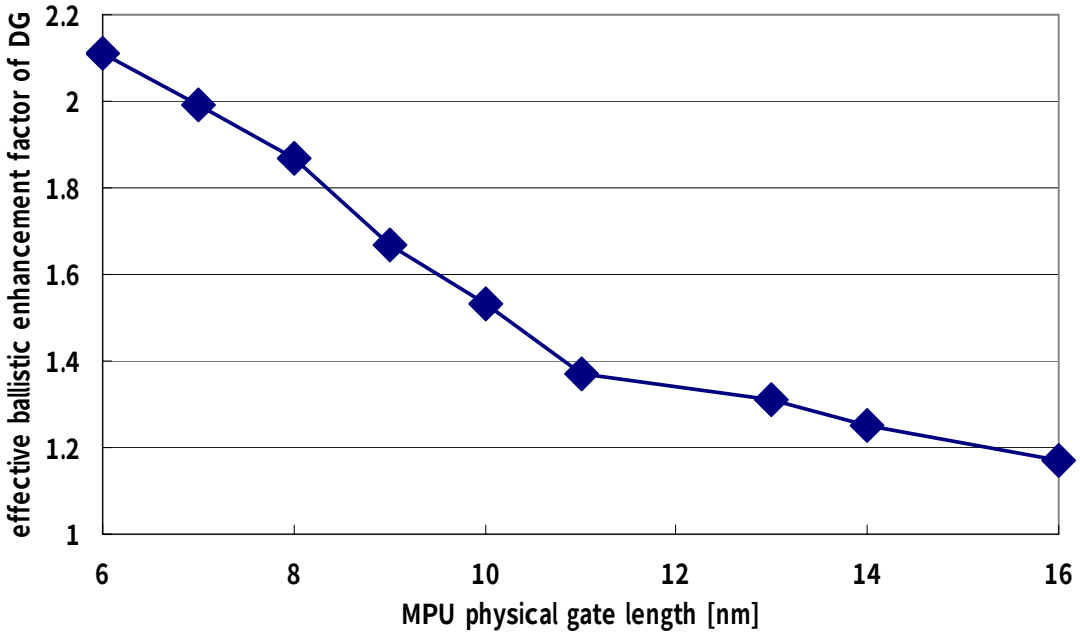

Figure 1.7 the gate length and the effect of ballistic conduction

Effective ballistic enhancement factor is about 1 in 2011 year but this factor exceeds 2 in 2020 year in figure 1.6. This shows that physical gate length becomes 6[nm] in 2020 year with figure 1.7 and ITRS predicts that ballistic conduction occurs often. The ballistic conduction is thought about as an important thing for future LSI, and now there is the necessity of the research.

1.4 RT model and research way of ballistic conductivity

About the research of the ballistic conductivity of MOSFET, there are approach of non equilibrium green function, Boltzmann transport equation, and a natural way for quantum mechanical effects. This last approach leads the ballistic drain current from state of a wave function. But real device need consider the scattering because real device does not become perfect ballistic. So reflection and transmission model (RT model) is made by K.Natori. RT model expresses reflection and transmission by scattering factor.

1.5 The electric potential of the channel and energy relaxation by optical phonon emission

Electrons moving from the source to the drain receive elastic scattering and inelastic scattering. Inelastic scattering emits the optical phonon while an electron loses energy. For an electron to loss the energy behind the bottle neck means that an electron can not exceed the bottle neck again even if an electron reflects by elastic scattering to the source side like figure 1.5. The electron can go only to a drain, and the drain current increases. This means that the structure of the electric potential of the channel strongly

affects a drain current. So there is necessity to search for the electric potential structure to increase the drain current.

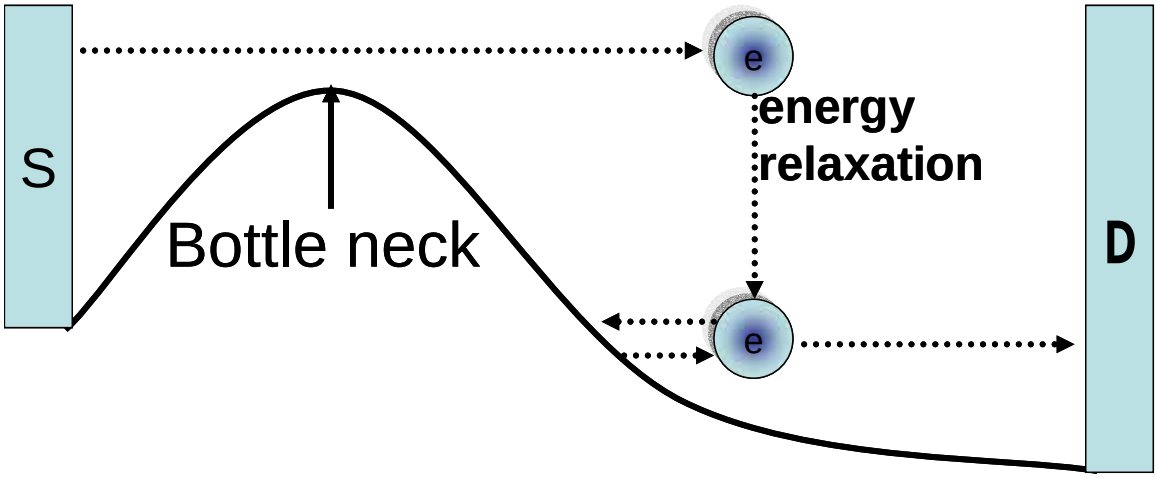

Figure 1.5 energy relaxation of electrons and shuttered electrons behind the bottle neck

1.6 The purpose of research

In this time, the purpose of research investigates the device structure to increase ballisticity by numerical calculation. In addition, to understand optical phonon emission in MOSFET, if the electric potential of the channel could be operated virtually, this research examines how its operation is connected with the optical phonon emission.

And chapter 4 introduces the research of high-k film by device simulator Taurus.

1.7 Reference

[1.1] by NCAD private corporation of “http://www.ncad.net/Co/mooreslaw_chart.gif”

[1.2] by George Watson, Univ. of Delaware, 1996 of

“http://www.physics.udel.edu/~watson/scen103/mos1.html”

[1.3] by xbitlaboratorys of

“http://www.xbitlabs.com/images/cpu/presler/lgate.jpg”

[1.4] Update 2006 table40 high performance logic technology

Chapter 2

Method

2.1 About RT model

RT model (reflection and transmission model) is the program of FORTRAN and expresses the current flow. This chapter explains RT model roughly. At firs, electrons from the source are injected. Electrons have kinetic energy of the thermal energy. Electrons of this energy pass each minute region of a source, channel and drain, and electrons receive scattering. Like figure 2.1, electrons injected to minute region of MOSFET express as total flux of 1, transmission flux of t, reflection flux of r and the flux of 1-t-r. The flux of 1-t-r loses energy by optical phonon emission.

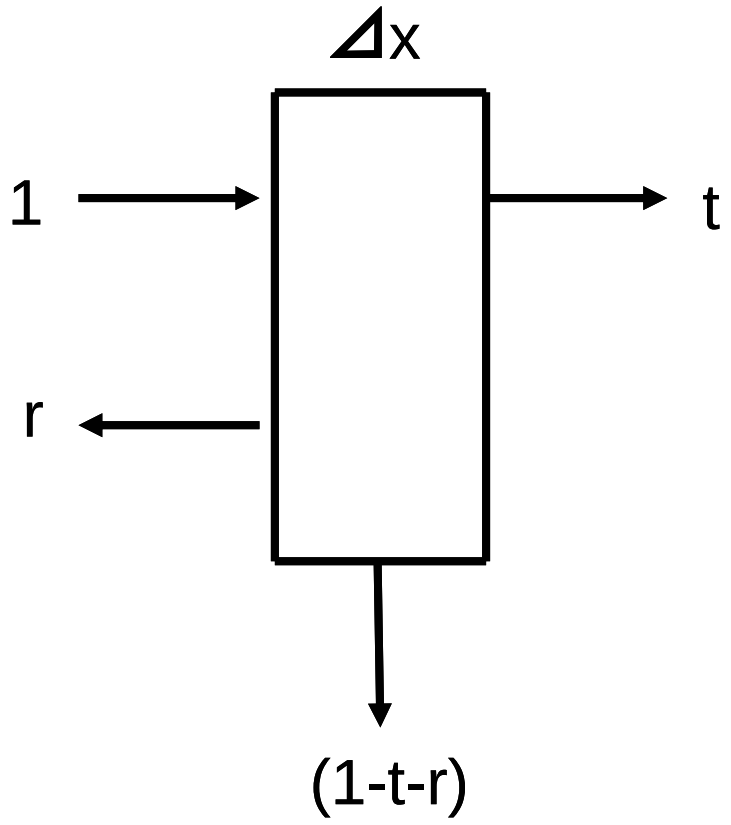

Figure 2.1 the flux from the left side in ⊿x of minute region

The flux of both sides of minute region can express as figure 2.2 when the flux from left side is f_1 and the flux from right side is f_4.

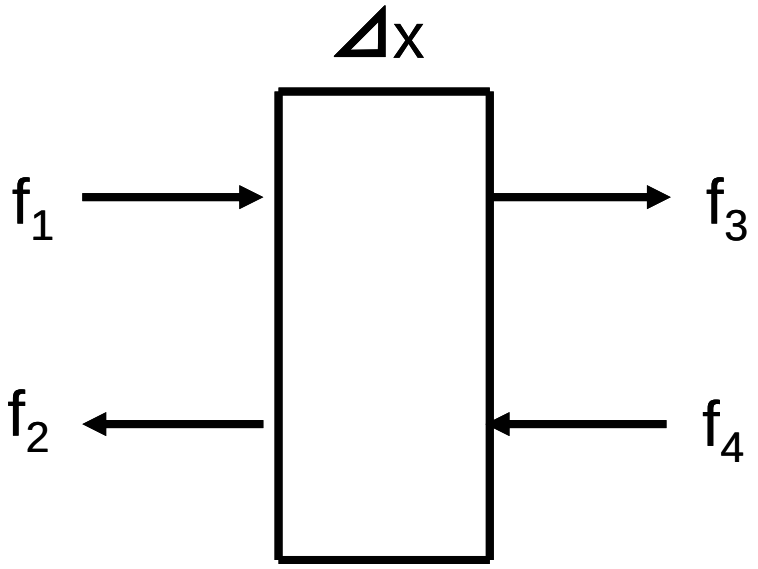

Figure 2.2 the flux from both sides in ⊿x of minute region

Here all flux by the optical phonon emission vanishes as approximation. And the matrix M which satisfies the next equation (1) (2) can be decided about f_1, f_2, f_3 and f_4.

$$\begin{pmatrix} f_3 \\ f_4 \end{pmatrix} = M \begin{pmatrix} f_1 \\ f_2 \end{pmatrix} \quad \text{.....(1)}$$

$$M = \begin{pmatrix} t_1 - \frac{r_1 r_2}{t_2} & \frac{r_2}{t_2} \\ -\frac{r_1}{t_2} & \frac{1}{t_2} \end{pmatrix} \quad \text{.....(2)}$$

Here the t_1 is probability of the transmission of the flux from left side. The r_1 is probability of the reflection of the flux from left side. The t_2 is probability of the transmission of the flux from right side. The r_2 is probability of the reflection of the flux from right side. Chapter 2-1-5 explains t_1, t_2, r_1 and r_2. The matrix of a large domain is made by multiplying the matrices of the minute domain. So a matrix can be decided by the four regions which is the source, the channel before bottle neck, the channel after

bottle neck and the drain. The bottle neck indicates the mountain of electric potential of the channel of figure1.5. Figure 2.3 expresses matrices and fluxes. s_3 and s_4 are flux on bottle neck like figure2.3. s_3 and s_4 are connected with s_5, s_6, f_s and f_D through the matrices of the channel. Here α_s and α_d are the ratio of the reflection of the flux from the source and the drain.

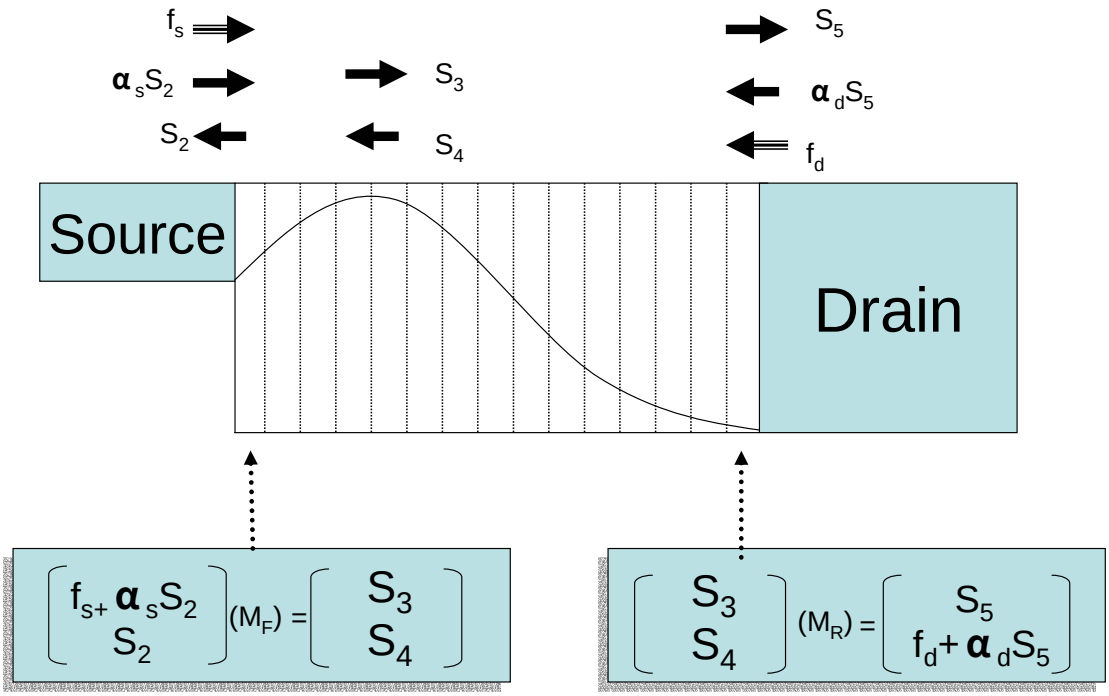

Figure 2.3 matrices of the minute region and fluxes

2.2 The physical model

There are the impurity scattering, the acoustic phonon scattering and the surface roughness scattering as the elastic scattering mainly. The impurity scattering is the scattering by the donor and the acceptor of the ionization. This uses Brooks Herring Model and Born approximation. The acoustic scattering is the scattering by the vibration of the lattice. The roughness scattering is the scattering by the unevenness of the gate insulator film. The inelastic scattering is the energy relaxation by the optical

phonon emission.

2.2.1 The impurity scattering

At first, the equation (3) is defined as the electric potential in the doping silicon.

$$V(r) = \frac{q^2}{4\pi\varepsilon r}\exp(-\lambda r) \quad \cdots\cdots (3)$$

Here q is an electric charge, ε is the dielectric constant and λ is the screening length. A differential scattering cross section is led by the equation (3).

$$\sigma(\theta) = \left(\frac{m}{2\pi\hbar^2}\right)^2 \left|\langle\psi_b|V(r)|\psi_a\rangle\right|^2 = \frac{d\sigma}{d\Omega} = \left(\frac{2mq^2}{4\pi\varepsilon\hbar^2}\right)\frac{1}{\left(K^2+\lambda^2\right)^2} \quad \cdots\cdots (4)$$

Here is the plank's constant, m is the electron mass, θ is an angle of scattering, $K = 2k\sin\frac{1}{2}\theta$ and k is the wave number. So the equation (5) of the mean free path is led by the equation (4).

$$\Lambda^{-1}(E) = 2\pi N_i \int_0^{\pi}(1-\cos\theta)\sigma(\theta)\sin\theta d\theta = \frac{\pi N_i}{2}\left(\frac{q^2}{4\pi\varepsilon}\frac{2m}{\hbar^2 k^2}\right)^2\left[\ln\left(1+4\frac{k^2}{\lambda^2}\right)-\frac{1}{1+\frac{\lambda^2}{4k^2}}\right] \quad \cdots\cdots (5)$$

Here N_i is the carrier density. The screening length λ is decided by the following. The screening by the carrier which is degeneration in three dimensions

$$\lambda = \left(\frac{6q^2\left(2m_t m_e\right)^{\frac{1}{2}}}{\varepsilon\pi^2\hbar^3}\right)^{\frac{1}{2}} E_F{}^{\frac{1}{4}} \quad \cdots\cdots (6)$$

The screening by the carrier which is no degeneration in three dimensions

$$\lambda = \sqrt{\frac{q^2}{\varepsilon_s}\frac{N_i}{k_B T}} \cdots\cdots (7)$$

Here T is temperature. So the mean free path is expressed as the equation (8).

$$\Lambda = 4.199785\times10^{-5}\frac{E^2}{N_i}\left[\ln\left(1+4\frac{E}{\Theta}\right)-\frac{1}{1+\frac{\Theta}{4E}}\right]^{-1} \cdots\cdots (8)$$

But Θ in the channel is the equation (9).

$$\Theta = 0.31026\left(\frac{N_i}{E}\right) \cdots\cdots (9)$$

Θ in the source and the drain is the equation (10).

$$\Theta = 1354.566(N_D) \cdots\cdots (10)$$

Here N_D is impurity density.

2.2.2 The acoustic phonon scattering

The acoustic phonon is approximated as the inelastic scattering. The scattering probability is expressed as the equation (11).

$$P = \frac{\sqrt{2}m^{\frac{3}{2}}k_B T\varepsilon_1^{\ 2}}{m\hbar^4 u_e^{\ 2}\rho}E^{\frac{1}{2}} = const\times E^{\frac{1}{2}} = \frac{1}{\tau} \cdots\cdots (11)$$

Here k_B is Boltzmann constant and τ is the relaxation time. The electronic velocity has next relation about the mean free path Λ.

$$\Lambda = v\tau$$
$$v = \sqrt{\frac{2E}{m}} = const'\times E^{\frac{1}{2}} \cdots\cdots (12)$$

When v and τ are substituted for the mean free path Λ, Λ is expressed as equation (13).

$$\Lambda = \frac{const'\times E^{\frac{1}{2}}}{const\times E^{\frac{1}{2}}} = const'' \cdots\cdots (13)$$

So the mean free path of the acoustic phonon is the constant. At this time, M.v.Fischetti et al and Phys.Rev.B 48 2244(1993) lead P＝4.5×10^{12}[s^{-1}]　and v=3.33×10^{7}[cm/s] in E＝60[meV], 300[K].[2.1] Λ is expressed as the equation (14) with the thermal dependency when this paper is grounded on.

$$\Lambda = 74\times\left(\frac{300}{T}\right)[nm] \quad \cdots\cdots (14)$$

2.2.3 The energy relaxation by optical phonon emission

The scattering probability is expressed as the equation (15) about the optical phonon emission.

$$P = \frac{(D_t K)^2 m^{\frac{3}{2}}}{2^{\frac{1}{2}}\pi\hbar^3\rho\omega_{op}}\left(E-\hbar\omega_{op}\right)^{\frac{1}{2}} = const\times\left(E-\hbar\omega_{op}\right)^{\frac{1}{2}} = \frac{1}{\tau} \quad \cdots\cdots (15)$$

Here ω_{op} is the frequency of the optical phonon and ω_{op} is 63[meV] in the silicon. The mean free path μ of the optical phonon emission and the velocity of the electron are expressed as the equation (16).

$$\mu = v\tau$$
$$v = \sqrt{\frac{2E}{m}} = const'\times E^{\frac{1}{2}} \quad \cdots\cdots (16)$$

By the equation (15) and (16),　μ is expressed as the equation(17).

$$\mu = \frac{const'\times E^{\frac{1}{2}}}{const\times\left(E-\hbar\omega_{op}\right)^{\frac{1}{2}}} = const''\times\frac{E^{\frac{1}{2}}}{\left(E-\hbar\omega_{op}\right)^{\frac{1}{2}}} \quad \cdots\cdots (17)$$

And M.v.Fischetti et al and Phys.Rev.B 48 2244(1993) lead P=2.0×10^{13}[s^{-1}] in E=0.3[eV]. [2.1] So μ is expressed as the equation (18).

$$\mu = 33.11\times\frac{E^{\frac{1}{2}}}{\left(E-\hbar\omega_{op}\right)^{\frac{1}{2}}}\,[\mathrm{nm}] \quad \cdots\cdots (18)$$

2.2.4 Surface roughness scattering

The relaxation time to lead the mean free path of surface roughness scattering is expressed as the equation (19).

$$\frac{1}{\tau} = \frac{2m_t q^2 {E_{eff}}^2}{\hbar^3} \Delta^2 L^2 \int_0^{\pi} \frac{(1-\cos\theta)d\theta}{\left[1+2L^2k^2(1-\cos\theta)\right]^{\frac{3}{2}}} \quad \cdots\cdots\cdots\cdots\cdots\cdots (19)$$

Here E_{eff} is a perpendicular electric field and $\Delta \cdot L$ is defined by the equation(20).

$$\left\langle \Delta(\vec{r}_1)\Delta(\vec{r}_2) \right\rangle = \Delta^2 \exp\left[-\frac{1}{L^2}(\vec{r}_1 - \vec{r}_2)^2 \right] \quad \cdots\cdots\cdots\cdots\cdots\cdots (20)$$

And total mean free path is composed by Matthiessen's rule like the equation(21).

$$\frac{1}{\lambda_{total}} = \frac{1}{\Lambda_{impurity}} + \frac{1}{\Lambda_{accoustic}} + \frac{1}{\Lambda_{roughness}} \quad \cdots\cdots\cdots\cdots\cdots\cdots (21)$$

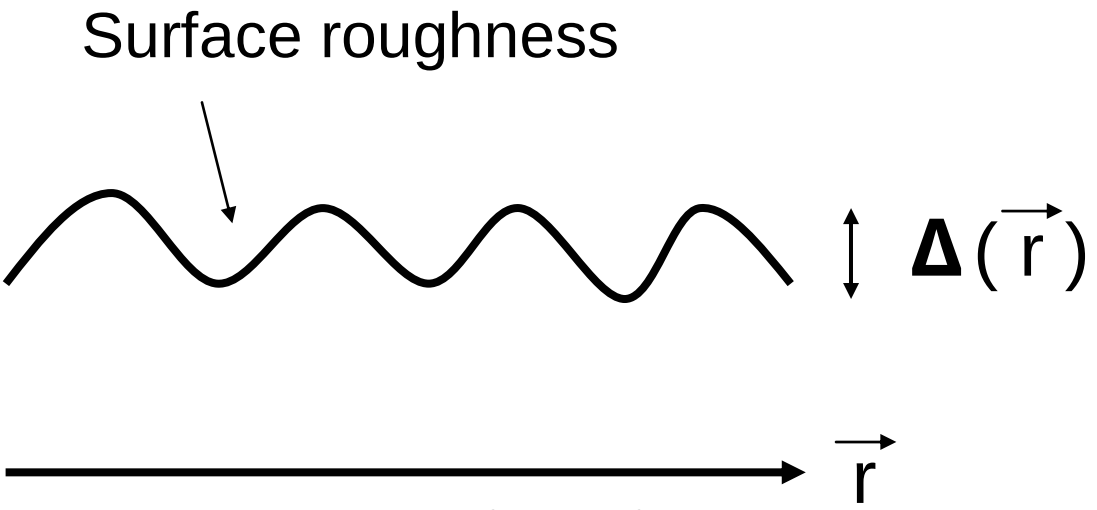

Figure 2.4 Δ and r of the surface roughness

2.2.5 The mean free path and probability of the transmission・reflection

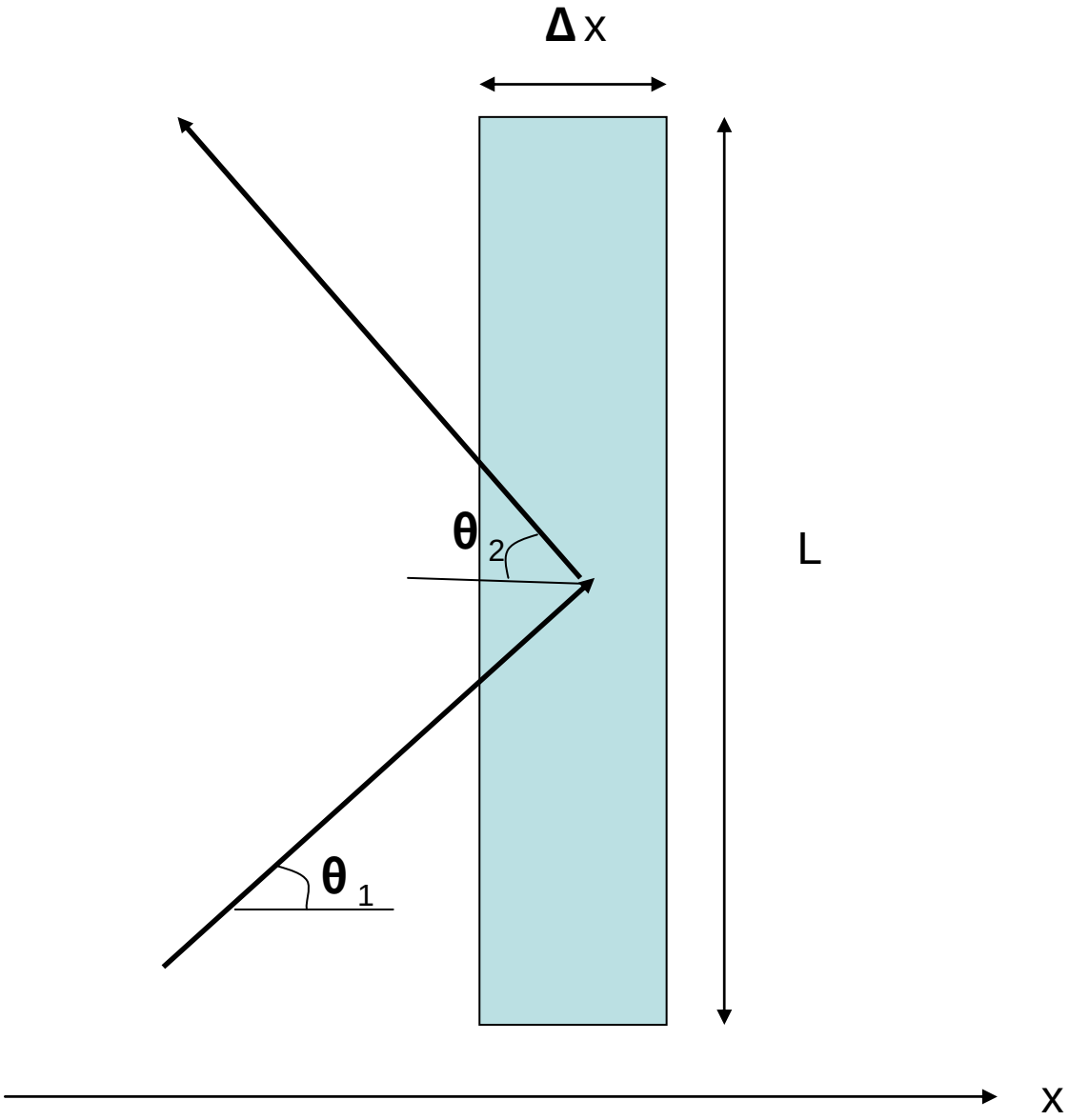

Figure 2.5 the flux which is incident on Δx and the flux which is scattered

An arrow of X axis is the drain direction from the source in figure2.5. Figure 2.5 shows incident flux and scattering flux in two dimensions. An arrow of θ_1 direction is incident flux which is expressed as vn(v). Here v is average velocity of the flux. In this time, total incident flux from the left is expressed as the equation (22).

$$\int_{-\frac{\pi}{2}}^{\frac{\pi}{2}} Lvn(v)\cos\theta_1 d\theta_1 = 2Lvn(v) \quad \cdots\cdots\cdots\cdots\cdots\cdots\cdots\cdots\cdots\cdots\cdots\cdots\cdots\cdots\cdots\cdots\cdots\cdots (22)$$

And when scattering probability is $S(\theta_1)$ in minute region, back scattering flux of the x direction is expressed as the equation(23).

$$\int_{-\frac{\pi}{2}}^{\frac{\pi}{2}} \frac{1}{2} LS(\theta_1) vn(v) \cos\theta_1 d\theta_1 \quad \cdots\cdots (23)$$

1/2 of the equation (23) shows that half fluxes scattered to all direction become the factor of the back scattering. And when electrons run the mean free path Λ, electrons are scattered in the probability of 1. In this time, S(θ) of the probability of the scattering is expressed as the equation (24).

$$S(\theta) = \frac{\Delta x}{\cos\theta_1} \frac{1}{\Lambda} \quad \cdots\cdots (24)$$

Δx is a minute region in comparison with the mean free path. So Λ is expressed as the equation (25).

$$\Lambda >> \frac{\Delta x}{\cos\theta_1} \quad \cdots\cdots (25)$$

And the back scattering flux is expressed as an equation (26) if S(θ1) is substituted for (23).

$$\int_{-\frac{\pi}{2}}^{\frac{\pi}{2}} \frac{1}{2} Lvn(v) \cos\theta_1 d\theta_1 \frac{\Delta x}{\cos\theta_1} \frac{1}{\Lambda} = vn(v) \frac{\pi}{2} \frac{\Delta x}{\Lambda} L \quad \cdots\cdots (26)$$

Because of (The probability of back scattering) = (the back scattering flux)/ (the incident flux), the probability of back scattering is expressed as the equation (27).

$$\frac{vn(v) \frac{\pi}{2} \frac{\Delta x}{\Lambda} L}{2vn(v)L} = \frac{\pi}{4} \frac{\Delta x}{\Lambda} \quad \cdots\cdots (27)$$

And the mean free path μ of the energy relaxation by the optical phonon emission is expressed as the equation (28) too.

$$S'(\theta) = \frac{\Delta x}{\cos\theta_1} \frac{1}{\mu} \quad \cdots\cdots (28)$$

The optical phonon emission need take out only back scattering probability but also probability of the transmission. So 1/2 of the equation (23) vanishes and the flux of the energy relaxation is expressed as the equation (29)

$$\int_{-\frac{\pi}{2}}^{\frac{\pi}{2}} \frac{1}{2} LS'(\theta_1) vn(v) \cos\theta_1 d\theta_1 \quad \cdots\cdots\cdots\cdots\cdots\cdots\cdots\cdots\cdots\cdots\cdots\cdots\cdots\cdots (29)$$

Because of (the probability of energy relaxation) = (the flux of the energy relaxation)/ (the incident flux), the probability of the energy relaxation is expressed as the equation (30).

$$\frac{\pi}{2}\frac{\Delta x}{\mu} \quad \cdots\cdots\cdots\cdots\cdots\cdots\cdots\cdots\cdots\cdots\cdots\cdots\cdots\cdots\cdots\cdots\cdots\cdots (30)$$

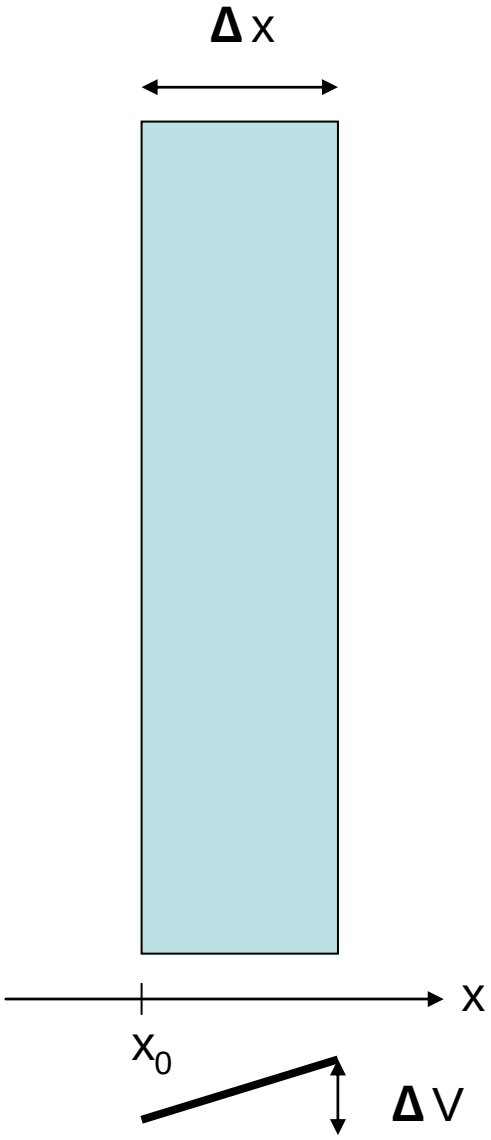

Figure 2.6 the incline of the electric potential ΔV in minute region Δx

Next consideration is the incline of the electric potential of ΔV in minute region Δx like figure 2.6.

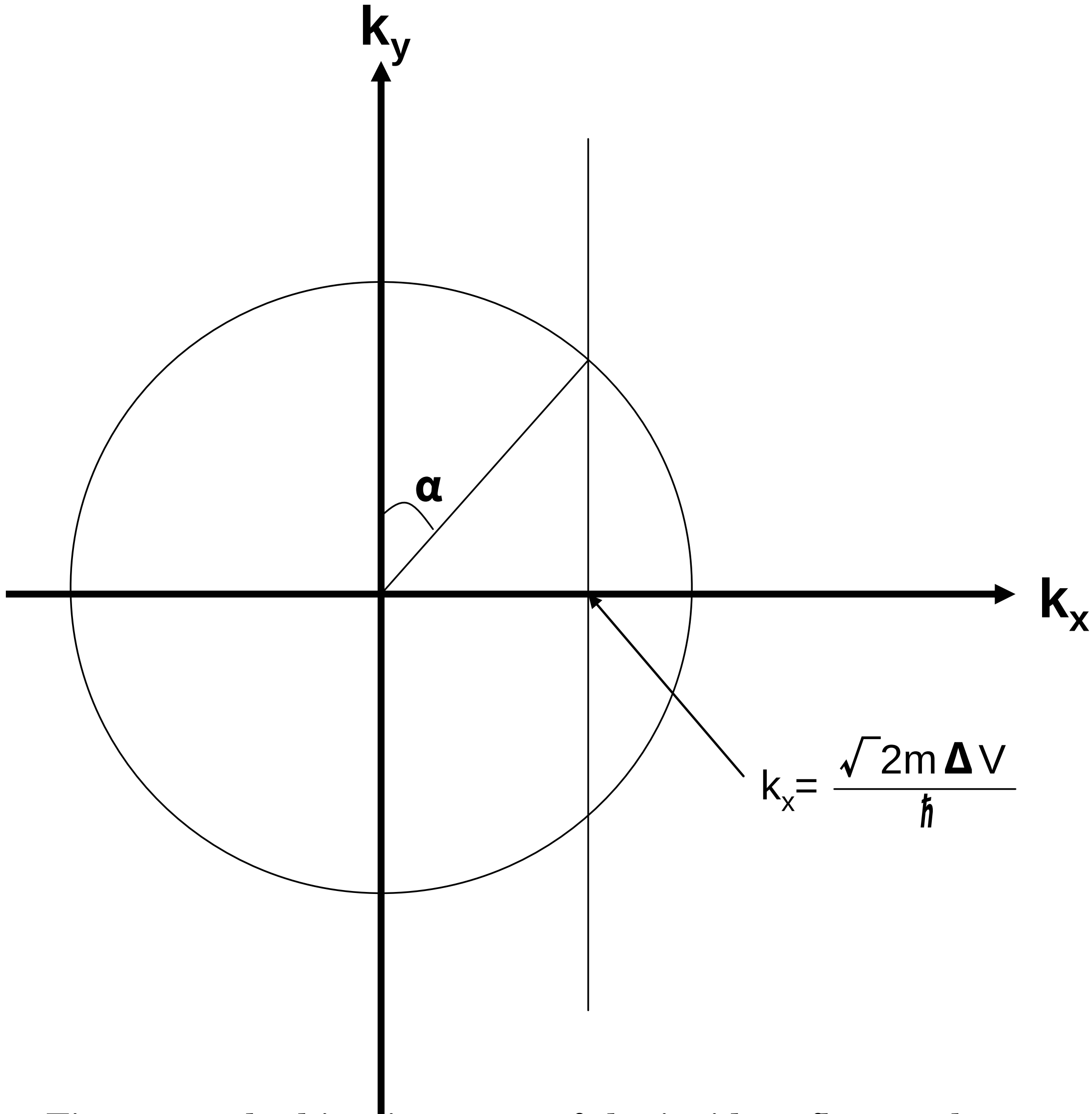

Figure 2.7 the kinetic energy of the incident flux on the wave number space and the critical angle of the reflection by the electric potential

Figure 2.7 expresses the kinetic energy on the wave number space and the critical angle of the reflection by electric potential. x direction of figure 2.7 is x direction of figure 2.6. In this time, kinetic energy of the wave number is expressed as the equation (31).

$$E = \frac{\hbar^2}{2m}\left(k_x{}^2 + k_y{}^2\right) \cdots\cdots (31)$$

$$k_x < \frac{\sqrt{2m\Delta V}}{\hbar} \cdots\cdots\cdots\cdots\cdots\cdots\cdots\cdots\cdots\cdots (32)$$

Carriers which suit the requirement of the equation (32) among the flux of the kinetic energy of the equation (31) cannot climb over the electric potential of ΔV because kinetic energy is smaller than ΔV. So the flux of the energy of the equation (32) do back scattering. The angle of α degree is the critical angle which reflects electrons by electric potential ΔV. Here θ is defined as a variable of the direction of α. Only flux of θ from 0 to π/2 can be considered because the circle is isotropic. Then only flux of θ from 0 to α does the back scattering. So the probability of back scattering is expressed as the equation (33).

$$\frac{\int_0^{\alpha} \sin\theta d\theta}{\int_0^{\frac{\pi}{2}} \sin\theta d\theta} = 1 - \cos\alpha = 1 - \sqrt{1 - \frac{\Delta V}{E}} \cdots\cdots\cdots\cdots\cdots\cdots\cdots\cdots (33)$$

The equation (33) is calculated by the equation (34). The equation (34) is led by figure 2.7.

$$\sin\alpha = \frac{k_x}{\sqrt{k_x{}^2 + k_y{}^2}} = \sqrt{\frac{\Delta V}{E}} \cdots\cdots\cdots\cdots\cdots\cdots\cdots\cdots (34)$$

The probability of the transmission is 1-(the probability of back scattering). So the equation (35) is led.

$$1 - \left(1 - \sqrt{1 - \frac{\Delta V}{E}}\right) = \sqrt{1 - \frac{\Delta V}{E}} \cdots\cdots\cdots\cdots\cdots\cdots\cdots\cdots (35)$$

On the other hand, when the electric potential drops to opposite direction of x direction, the back scattering does not occur. So in this time, the probability of the transmission is 1.

From an above-mentioned argument, the probability of the transmission with the

electric potential barrier is expressed as the equation (36).

$$t_1 = -0.785398\frac{\Delta x}{\Lambda(E)} + \sqrt{1-\frac{\Delta V}{E}} - 1.570796\frac{\Delta x}{\mu(E)} \quad \cdots\cdots\cdots\cdots\cdots\cdots (36)$$

The probability of the reflection with the electric potential barrier is expressed as the equation (37).

$$r_1 = 0.785398\frac{\Delta x}{\Lambda(E)} + \left(1-\sqrt{1-\frac{\Delta V}{E}}\right) \quad \cdots\cdots\cdots\cdots\cdots\cdots\cdots\cdots (37)$$

The probability of the transmission without the electric potential barrier is expressed as the equation (38).

$$t_2 = 1 - 0.785398\frac{\Delta x}{\Lambda(E)} - 1.570796\frac{\Delta x}{\mu(E)} \quad \cdots\cdots\cdots\cdots\cdots\cdots\cdots (38)$$

The probability of the reflection without the electric potential barrier is expressed as the equation (39).

$$r_2 = 0.785398\frac{\Delta x}{\Lambda(E)} \quad \cdots\cdots\cdots\cdots\cdots\cdots\cdots\cdots\cdots (39)$$

These equations become the grounds of the equation (2). And the ballistic drain current on the surface of Si(100) is expressed by multi sub band model(MSM) as the equation(40).

$$I_D = W\frac{\sqrt{2}q(k_BT)^{\frac{3}{2}}}{\pi^2\hbar^2}\sum_{valley}\sum_{n}\sqrt{m_y}\times\left[F_{1/2}\left(\frac{\phi_{FS}-E_n}{k_BT}\right)-F_{1/2}\left(\frac{\phi_{FS}-E_n-qV_D}{k_BT}\right)\right] \quad \cdots\cdots (40)$$

And an electric charge on the source edge is expressed as the equation (41).

$$|Q| = C(V_G - V_t)$$
$$= \frac{qk_BT}{2\pi\hbar^2}\sum_{valley}\sum_{n}\sqrt{m_x m_y}\ln\left\{\left[1+\exp\left(\frac{\phi_{FS}-E_n}{k_BT}\right)\right]\left[1+\exp\left(\frac{\phi_{FS}-E_n-qV_D}{k_BT}\right)\right]\right\} \quad \cdots\cdots (41)$$

Here, V_G,V_D and V_t are respectively the gate bias, the drain bias and the threshold voltage, W is the channel width, |Q| is the channel charge density at the source edge, q

is the elementary charge, m_x(m_y) is the electron effective mass along (across) the channel, and φ_{FS} is the Fermi level of the source electrode. Here Fermi-Dirac integral is defined as the equation (42).

$$F_{1/2}(u) = \int_0^\infty \frac{\sqrt{y}}{1+\exp(y-u)} dy \quad \cdots\cdots\cdots\cdots\cdots\cdots\cdots\cdots\cdots\cdots\cdots\cdots (42)$$

2.3 The general constitution of program

At first, the profiling of the electric potential of the channel need be defined. Then the matrix of the equation (2) can be calculated because the profiling of the electric potential leads t and r by the equation (36) (37) (38) (39). The matrix of a large domain is made by multiplying matrices of the minute region. So a matrix can be decided by the four regions which is the source, the channel before bottle neck, the channel after bottle neck and the drain. Here the matrix of the source is defined as M_S, the matrix of the channel before bottle neck is defined as M_F, the matrix of the channel after bottle neck is defined as M_R and the matrix of the drain is defined as M_D. The flux from the source edge to the channel is defined as s_1 and the flux from the channel to the source edge is defined as s_2. The equation (43) is the state of the flux of the source region. The right side of the equation (43) is the flux of the source electrode.

$$M_s^{-1}\begin{pmatrix} s_1 \\ s_2 \end{pmatrix} = \begin{pmatrix} 0 \\ \approx 0 \end{pmatrix} \quad \cdots\cdots\cdots\cdots\cdots\cdots\cdots\cdots\cdots\cdots\cdots\cdots\cdots (43)$$

The equation (43) can lead the relation of between s_1 and s_2. Then the equation (44) of the rate of the reflection is led from s_1 and s_2.

$$\alpha_s = \frac{s_1}{s_2} \quad \cdots\cdots\cdots\cdots\cdots\cdots\cdots\cdots\cdots\cdots\cdots\cdots\cdots\cdots\cdots (44)$$

Same expression in the drain side is possible. The rate of reflection in the drain is

expressed as the equation (45).

$$\alpha_D = \frac{s_6}{s_5} \quad \cdots\cdots (45)$$

Here s_5 is the flux from the channel to the drain edge. s_6 is the flux from the drain edge to the channel. The right side of the equation (43) is zero because another incident flux in the source is defined as ballistic flux as follows. s_{30} of the ballistic flux from the source to the drain and s_{40} of the ballistic flux from the drain to the source are defined by multi sub band model(MSM) as the equation (46) and (47) when the width of the channel is W=1[μm].

$$s_{30} = \frac{\sqrt{2}(k_B T)^{\frac{3}{2}}}{\pi^2 \hbar^2} \sum_{valley} \sum_{nz} \sqrt{m_y} \times \left[F_{\frac{1}{2}} \left(\frac{\Delta\phi - (E_{nz} - E_{0z})}{k_B T} \right) \right] \quad \cdots\cdots (46)$$

$$s_{40} = \frac{\sqrt{2}(k_B T)^{\frac{3}{2}}}{\pi^2 \hbar^2} \sum_{valley} \sum_{nz} \sqrt{m_y} \times \left[F_{\frac{1}{2}} \left(\frac{\Delta\phi - (E_{nz} - E_{0z}) - qV_D}{k_B T} \right) \right] \quad \cdots\cdots (47)$$

Here the equation (48) is assumed on trial.

$$\phi_{FS} - E_{0z} = \Delta\phi \quad \cdots\cdots (48)$$

And the quantity Q_{30} of electric charge by s_{30} expressed as the equation (49).

$$Q_{30} = \frac{q k_B T}{2\pi\hbar^2} \sum_{valley} \sum_{nz} \sqrt{m_x m_y} \ln\left[1 + \exp\left(\frac{\Delta\phi - (E_{nz} - E_{0z})}{k_B T} \right) \right] \quad \cdots\cdots (49)$$

The quantity Q_{40} of electric charge by s_{40} expressed as the equation (50).

$$Q_{40} = \frac{q k_B T}{2\pi\hbar^2} \sum_{valley} \sum_{nz} \sqrt{m_x m_y} \ln\left[1 + \exp\left(\frac{\Delta\phi - (E_{nz} - E_{0z}) - qV_D}{k_B T} \right) \right] \quad \cdots\cdots (50)$$

The velocity of the flux is expressed as the equation (51) (52) by the equation (46) (47) (49) (50).

$$v_3 = \frac{qs_{30}}{Q_{30}} = \frac{2\sqrt{2}\sqrt{k_B T}}{\pi\sqrt{m_x}} \frac{\sum_{valley}\sum_{nz} F_{1/2}\left(\frac{\Delta\phi - (E_{nz} - E_{0z})}{k_B T}\right)}{\sum_{valley}\sum_{nz} \ln\left[1 + \exp\left(\frac{\Delta\phi - (E_{nz} - E_{0z})}{k_B T}\right)\right]} \quad \cdots\cdots\cdots\cdots (51)$$

$$v_4 = \frac{qs_{40}}{Q_{40}} = \frac{2\sqrt{2}\sqrt{k_B T}}{\pi\sqrt{m_x}} \frac{\sum_{valley}\sum_{nz} F_{1/2}\left(\frac{\Delta\phi - (E_{nz} - E_{0z}) - qV_D}{k_B T}\right)}{\sum_{valley}\sum_{nz} \ln\left[1 + \exp\left(\frac{\Delta\phi - (E_{nz} - E_{0z}) - qV_D}{k_B T}\right)\right]} \quad \cdots\cdots\cdots (52)$$

The incident flux from the source to the drain is defined as f_s. Then the ballistic flux of between the bottle neck and source edge expressed as the equation (53).

$$M_F^*\begin{pmatrix} f_s \\ s_{20} \end{pmatrix} = \begin{pmatrix} s_{30} \\ s_{40} \end{pmatrix} \quad \cdots\cdots\cdots\cdots\cdots\cdots\cdots\cdots\cdots\cdots\cdots\cdots (53)$$

The matrix of the equation (53) leads the simultaneous equations. So f_s is led by s_{30} and s_{40}. Here the equation of s_{20} is ignored. f_D of incident flux from the drain to the channel is led by the equation of the matrix too. The fs from the source and the f_D from the drain are defined as no ballistic incident flux. Then the flux of the bottle neck is expressed as the equation (54) (55) by M_F and M_R.

$$M_F\begin{pmatrix} f_s + s_1 \\ s_2 \end{pmatrix} = \begin{pmatrix} s_3 \\ s_4 \end{pmatrix} \quad \cdots\cdots\cdots\cdots\cdots\cdots\cdots\cdots\cdots\cdots\cdots\cdots (54)$$

$$M_R\begin{pmatrix} s_3 \\ s_4 \end{pmatrix} = \begin{pmatrix} s_5 \\ f_D + s_6 \end{pmatrix} \quad \cdots\cdots\cdots\cdots\cdots\cdots\cdots\cdots\cdots\cdots\cdots\cdots (55)$$

Matrices of the equation (54) (55) lead four equation. s_3 and s_4 can be expressed in only α_s, α_D, f_s and f_D by these equation. And s_3, s_4, v_3 and v_4 lead the equation (56).

$$Q = q\left(\frac{s_3}{v_3} + \frac{s_4}{v_4}\right) \quad \cdots\cdots\cdots\cdots\cdots\cdots\cdots\cdots\cdots\cdots\cdots\cdots (56)$$

Here v_3 and v_4 are the same as ballistic velocity of electrons approximately.

$$Q = C_{eff}(V_G - V_t) \cdots \cdots (57)$$

The agreement of the equation (56) and (57) is checked. If two equations is not same value, Δφ of the equation (48) is assumed on trial again and the equation (56) is led again. This cycle is repeated until the equation (56) and (57) become same value. Q, f_s and f_D decrease when Δφ becomes small. The solution of Q is led by Newton's method because Δφ is monotonic function. Then the s3 and s4 is decided automatically. So the drain current is led by the equation (58).

$$I_D = q(s_3 - s_4) \cdots \cdots (58)$$

2.4 The device simulator Taurus

Taurus is device simulator soft of synopsys company. Taurus software consists of Taurus process, Taurus device and Taurus visual. Each this software is explained in this chapter. In this time, the possibility to operate the channel electric potential by doping is inspected as consideration of RT model, and analysis of FinFET with high-k film is performed by Taurus. The following makes extracts from the introduction of the taurus by the Taurus manual [2.2].

2.4.1 Taurus process

Taurus-Process is process simulator for one-, two-, and three-dimensional structure. Taurus-process simulates the fabrication steps used to manufacture semiconductor devices. Simulation capabilities are focused on frontend processes such as ion implantation, dopant activation, and annealing including oxidation and silicide growth. The simulator allows the specification of arbitrary initial geometries. The simulation of

etching and deposition is restricted to simple geometric operation where the resulting shape can be derived from the initial structure and the process description. Current, Taurus-Process does not offer capabilities for simulating the physics and chemistry of etching and deposition processes.

Taurus-Process allows you to:

Simulate 1D, 2D, and 3D structures and impurity profiles generated during the fabrication process.

Analyze the mechanical stresses that develop during processing.

Automatically adapt the mesh during the course of the process simulation.

Specify and use new equation and models during the process simulation.

2.4.2 Taurus device

Major Features

The main features of Taurus-Device include:

Multi-Dimension Device Simulation

Mesh Generation

Advanced Physical Models

Advanced Analysis Capabilities

Advanced Numerical Methods

Physical Model and Equation Interface

Multi-Dimensional Device Simulation

Taurus-Device simulates the electrical and thermal behavior of a wide range of semiconductor devices in one, two, and three-dimensions. Structures can be constructed by using simple boundary descriptions or by physical process simulation via the interface to Synopsys process simulators. The investigation of 3D phenomena (e.g., channel length/width dependencies, breakdown, and parasitic effects) can be accomplished quickly and easily.

Coordinate System

Taurus-Device uses a left-handed coordinate system. The Y-axis points into the wafer, and the layout plane is X-Z. Only Y-coordinates are used in all simulations in 1D, 2D, and 3D. The X-axis points to the right. X-coordinates are used in 2D and 3D simulations only in 3D simulation.

All coordinates, lengths, and thicknesses can be specified with a length unit; otherwise, the input values are assumed to be in µm. The internally used length scale is cm. 1D simulations are performed along the line through X=0, Z=0 and 2D simulations are performed in the plane Z=0. The user can specify the initial position of the substrate surface and the crystal orientation. By default, a <100> oriented substrate is assumed.

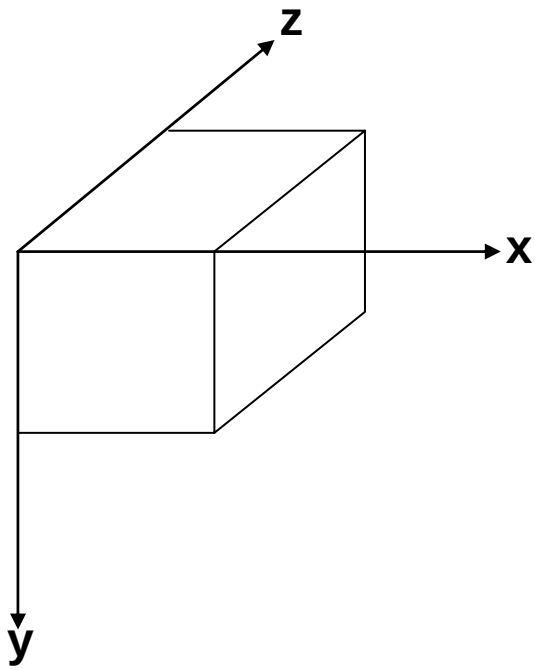

Figure 2.8 three-dimensional space of the Taurus

Mesh Generation

Efficient, automatic mesh generation greatly facilitates structure creation and device simulation in Taurus-Device. Quadtree/octree mesh generation provides optimal grids for accurate simulation results using a minimum number of mesh points. Advanced features including refinement and unrefinement, anisotropic refinement, boundary layers, and a level set boundary condition allow the construction of optimal meshes for any type of structure.

Advanced Physical Models

Taurus-Device can solve several types of equations using a wide variety of physical models. Some of the equations and models that can be used are listed below:

Equations Equations include the following:

Drift-diffusion equations

Heat equation for analysis of thermal effects

Hydrodynamic equations for the analysis of deep submicron devices

Conductance equation for the analysis of current flow in interconnects

Models Models include the following:

Complete set of mobility models that include many scattering phenomena and high-field effects

Boltzmann and Fermi-Dirac statics as well as models for the incomplete ionization of impurities

Complete set of recombination models including SRH, Auger, and direct recombination

Self-consistent impact ionization model for breakdown simulation

Self-consistent Band-to-Band tunneling models

Fowlet-Nordheim tunneling and hot carrier injection models

Quantum correction models including the van Dort and MLDA models and a Schrodinger equation solver

Direct tunneling models

Stress-induced bandgap and mobility models

Lumped and distributed elements models for resistance, capacitance, and inductance

Heterojunction models for compound semiconductor devices

Advanced Analysis Capabilities

Taurus-Device contains a wide variety of analysis capabilities:

Mixed-mode circuit simulation including support for BSIM3v3 and HSPICE compact models

Solution with voltage or current boundary condition at contacts

DC, transient, small-signal AC, and large-signal cyclic-bias analysis

Continuation method for the automatic tracing of I-V curves

Photogeneration and raytracing for optical devices

Advanced Numerical Methods

Taurus-Device contains a wide variety of numerical solvers and algorithms for improving convergence:

Fast direct and iterative linear solvers

Flexible equation coupling scheme

Physical Model and Equation Interface

The built-in Physical Model and Equation Interface (PMEI) allows for easy and flexible definition of new physical models and partial differential equations. Using the PMEI, you can run simulations using your own set of models and equations. Areas of particular utility include mobility, impact ionization, and hot carrier modeling. This tool is equally applicable to all partial differential equation simulations.

The solution method is fully controlled by you. For example, all available or user-defined equations can be solved individually, iteratively coupled, or fully coupled. PMEI is optionally available from Synopsys TCAD Business Unit. Contact the TCAD representative in your area for additional information.

2.4.3 Taurus visual

By overview of Taurus Visual

You can use Taurus Visual to create plots that display fields, geometries, and regions, including results such as P/N junctions and depletion layers. Taurus Visual allows you to view I-V curves and doping profiles and provide tools to zoom, pan, and rotate images. You can also extract data using rulers and probes. You can annotate plots with labels, lines and legends, and then print or save to a file.

The graphical user interface (GUI) provides direct and easy to use operations, as well as advanced controls for expert users. With the Taurus Visual GUI, you can systematically visualize devices in 1D, 2D, and 3D. Taurus visual executables include the following:

tv for visualizing 3D simulation data

tv2d for visualizing 2D simulation data

tv1d for visualizing 1D simulation data

2.5 Reference

[2.1]M.v.Fischetti et al and Phys.Rev.B 48 2244(1993)

[2.2] “Taurus manual” of synopsys company

Chapter 3

Result of RT model

3.1 The dope concentration of the channel

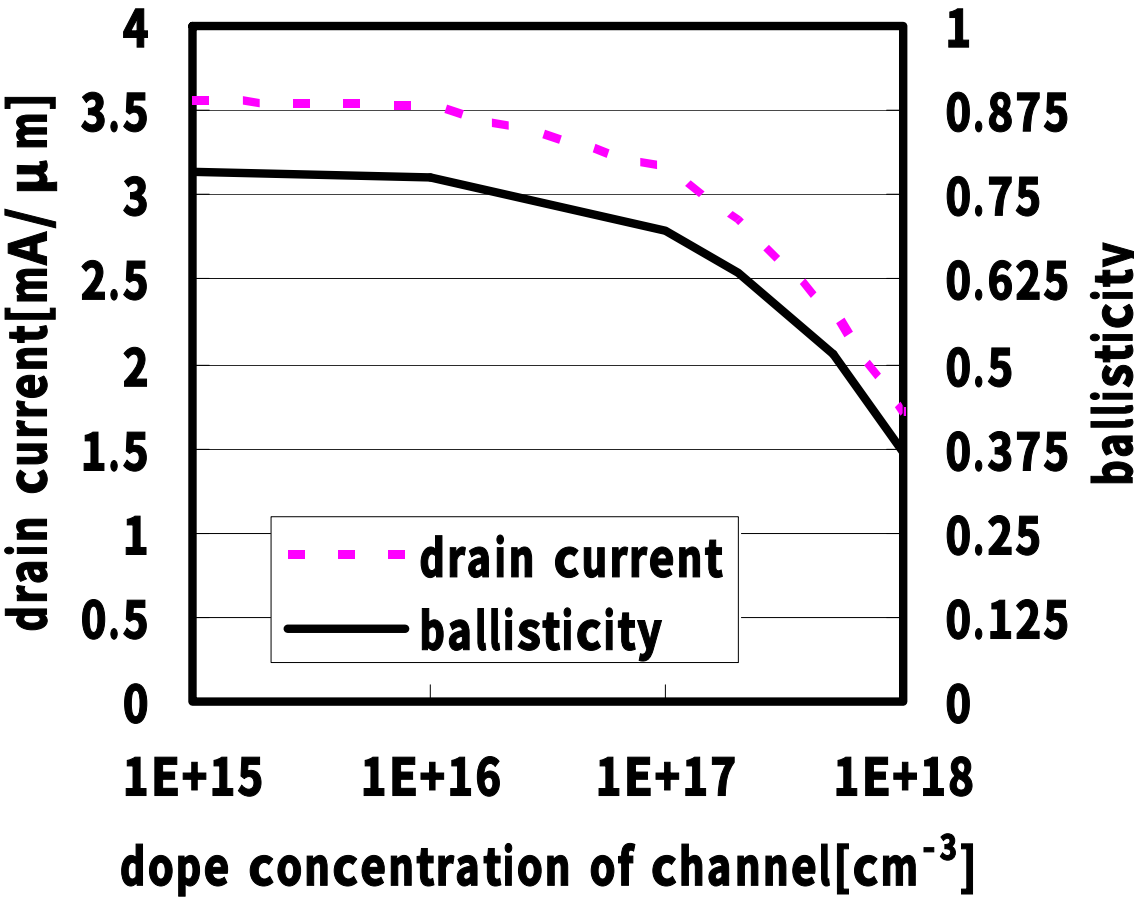

Figure 3.1 ballisticity and dope concentration of the channel

Figure3.1 shows the calculated channel doping concentrations dependency of the ballisticity in a MOSFET with Lg=10[nm] and tox=0.5[nm] at Vg=0.5[V] and Vd=0.6[V]. The drain doping concentration was set to be 1×10^{20}[cm^{-3}] in the calculation. Figure3.1 shows the ballisticity increases with channel doping concentration decreases. Higher ballisticity was obtained when the channel doping is low. The calculated ballisticity was 0.4 when channel doping concentration is 10^{18}[cm^{-3}], but with the decreasing of the channel doping concentration, ballisticity reaches higher than 0.75 when the channel doping concentrations are below 10^{16}[cm^{-3}].

3.2 The dope concentration of the drain with the ballistic channel

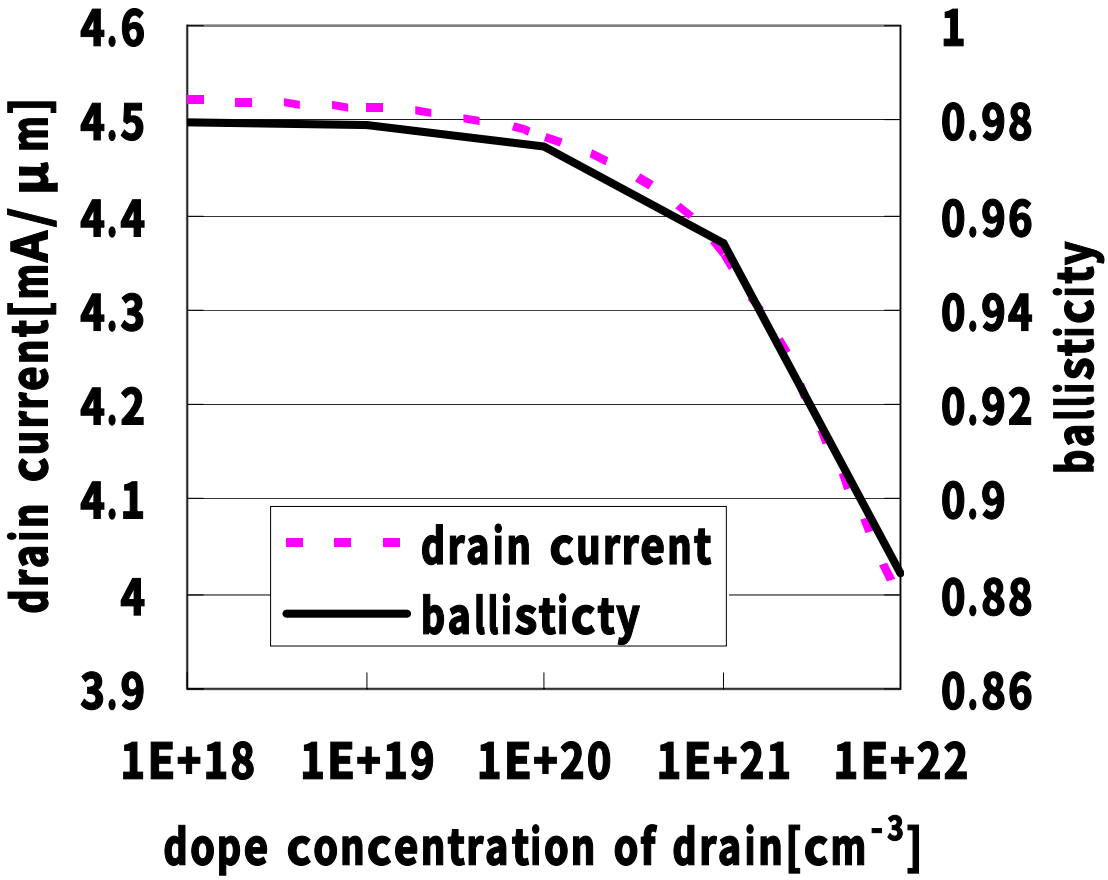

Figure 3.2 ballisticity and dope concentration of the drain

But even if the scattering of the channel become few, the problem remains. It is back scattering of the drain. Back scattering means reflection of electrons from the drain. The effect of back scattering of the drain need be investigated. Here to see only the influence of the back scattering of the drain, the channel is ballistic. Figure 3.2 shows the calculated drain doping concentration dependency of the ballisticity in a MOSFET with Lg=10[nm], tox=0.5[nm] and extension=5[nm] at Vg=0.5[V] and Vd=0.6[V]. Obtained results show that for higher ballisticity, low drain doping concentrations (lower than 10^{20}[cm^{-3}]) are preferred.

3.3 The length of the extension with the ballistic channel

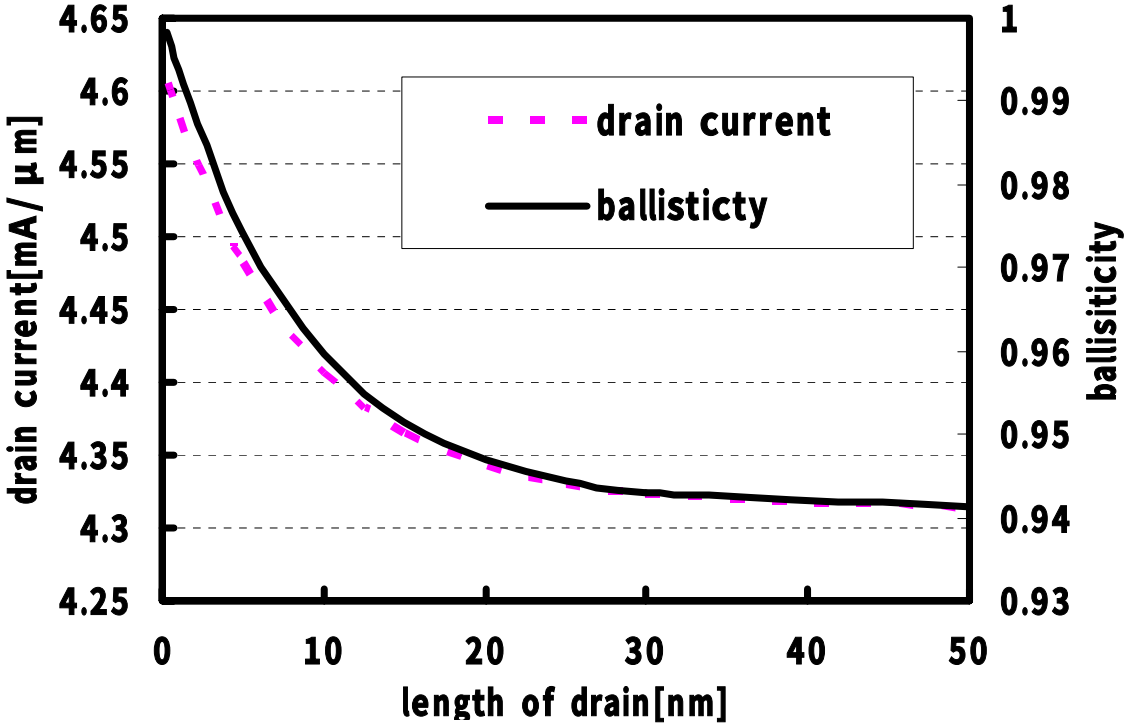

Figure 3.3 ballisticity and the length of the extension of the drain

Figure 3.3 is the length of the extension vs the drain current and the ballisticity in Vg=0.5[V], Vd=0.6[V], tox=0.5[nm],the dope concentration of the channel=9×10^{18}[cm^{-3}] and the dope concentration of the drain =1×10^{20}[cm^{-3}], Lg=10[nm] when channel is ballistic. This shows that extension less than 20[nm] increases the ballisticity, if the drain electrode absorbs electrons. On the contrary, more than 20nm become the stable state.

3.4 The ratio of the mean free path of elastic scattering and inelastic scattering

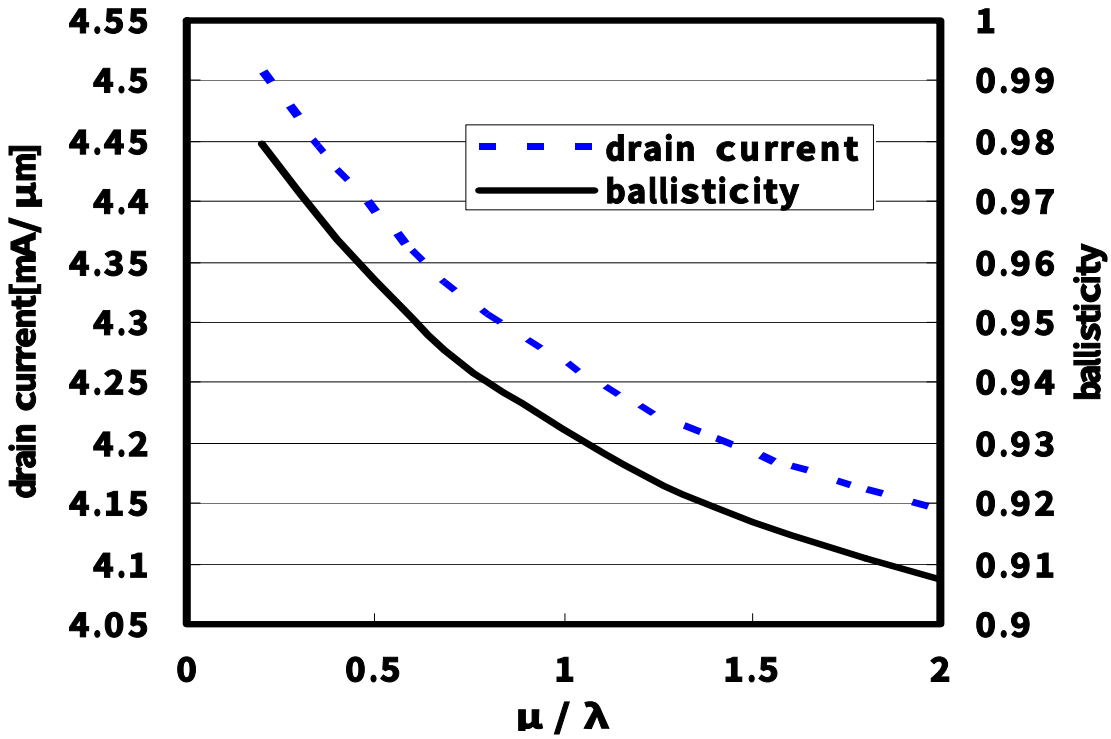

Figure 3.4 ballisticity and rate of mean free path of elastic scattering and inelastic scattering

Since the inelastic scattering mediated by optical phonons is the energy relaxation process of the electrons, it is an important factor for ballisticity because the electrons reached to the drain region may loose their energy by inelastic scattering and cannot return to the source when reflected by the drain. Using the ratio of the mean free path of inelastic scattering (μ) and the mean free path of elastic scattering (λ), we calculated ballisticity and drain current in a MOSFET with Lg=10[nm], tox=0.5[nm] and extension=5[nm] under the conditions of λ=10[nm], Vg=0.5[V], Vd=0.6[V], channel full ballistic and drain doping concentration =1×10^{20}[cm^{-3}]. Calculated results are shown in the Figure 3.4. The drain current and the ballisticity increase with the decreasing of the mean free path of inelastic scattering, in the other words, the drain current and the ballisticity increase with the increase of inelastic scattering.

3.5 The relation of elastic scattering and inelastic scattering

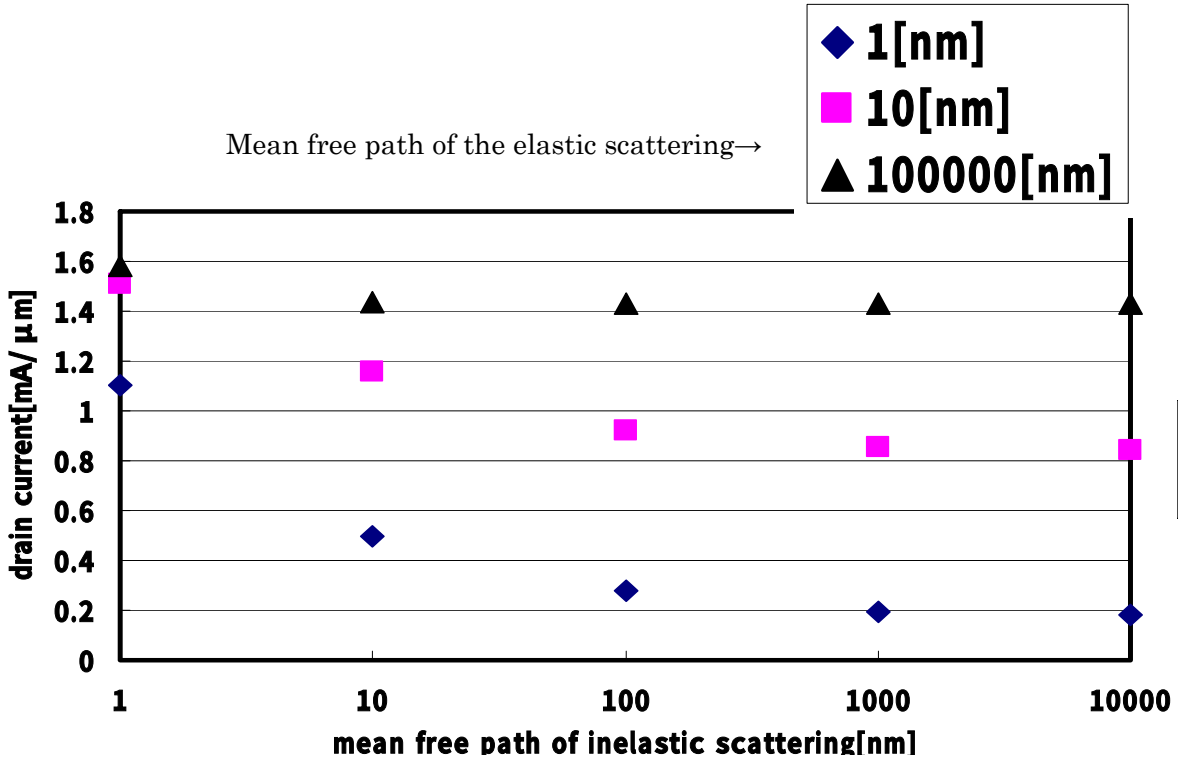

Figure 3.5 the relation of elastic scattering and inelastic scattering

Effects of the mean free path of elastic and inelastic scattering on drain currents are shown in the Figure 3.5. The calculation was carried out using a MOSFET with Lg=5.6[nm], and tox=1.5[nm] under the conditions of Vg=0.5[V], Vd=0.6[V], channel doping concentration =$1x10^{18}$[cm^{-3}] and drain doping concentration =$1x10^{20}$[cm^{-3}] by varying mean free path of elastic and inelastic scattering. Calculated drain current does not change while the mean free path of inelastic scattering changed from 1nm to 10,000nm when the mean free path of elastic scattering is long. But when the mean free path of elastic scattering become short, drain currents increase with the decreasing of the mean free path of inelastic scattering.

3.6 The influence of the drain current by electric potential of the channel

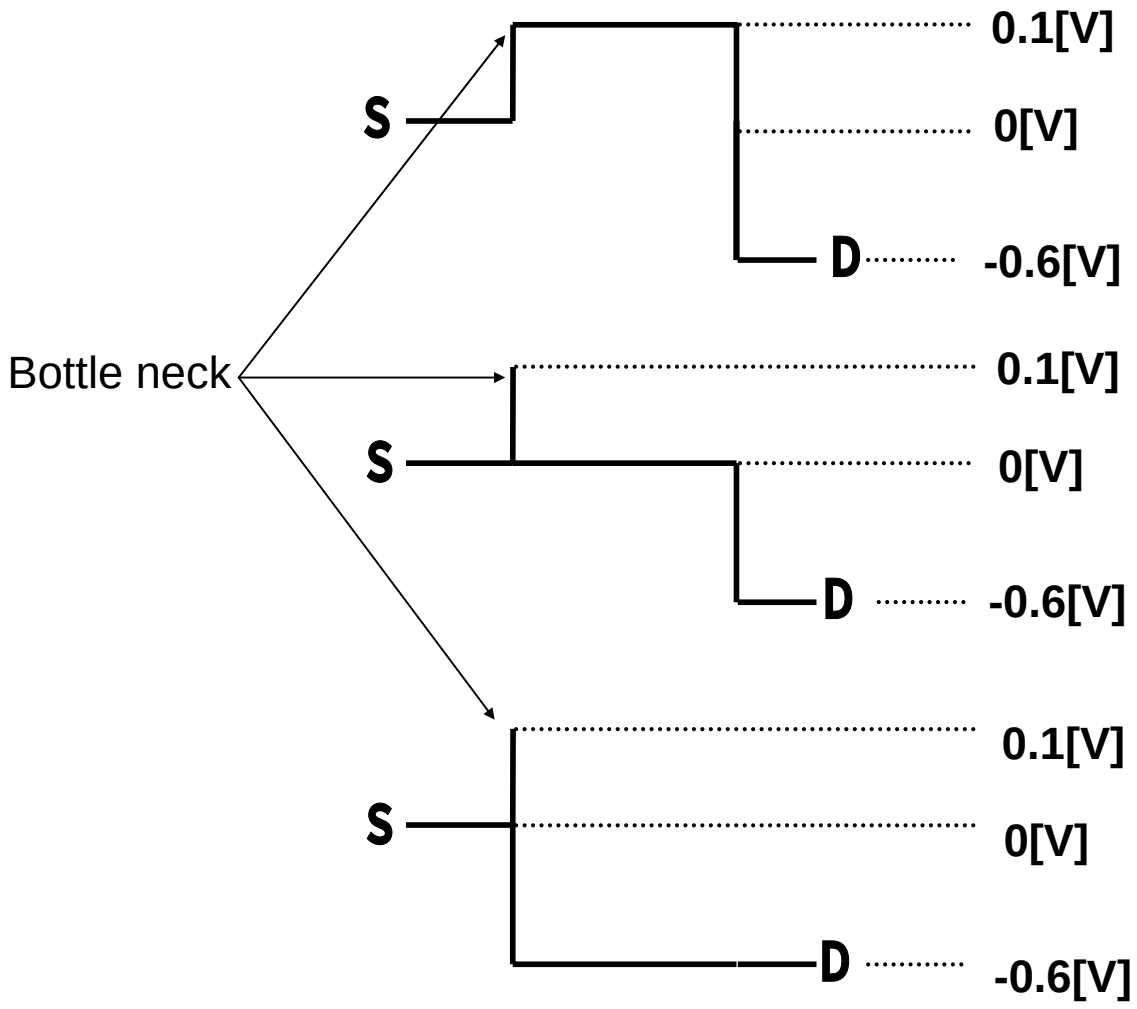

Figure 3.6 the pattern 1 of the position of channel electric potential behind the bottle neck

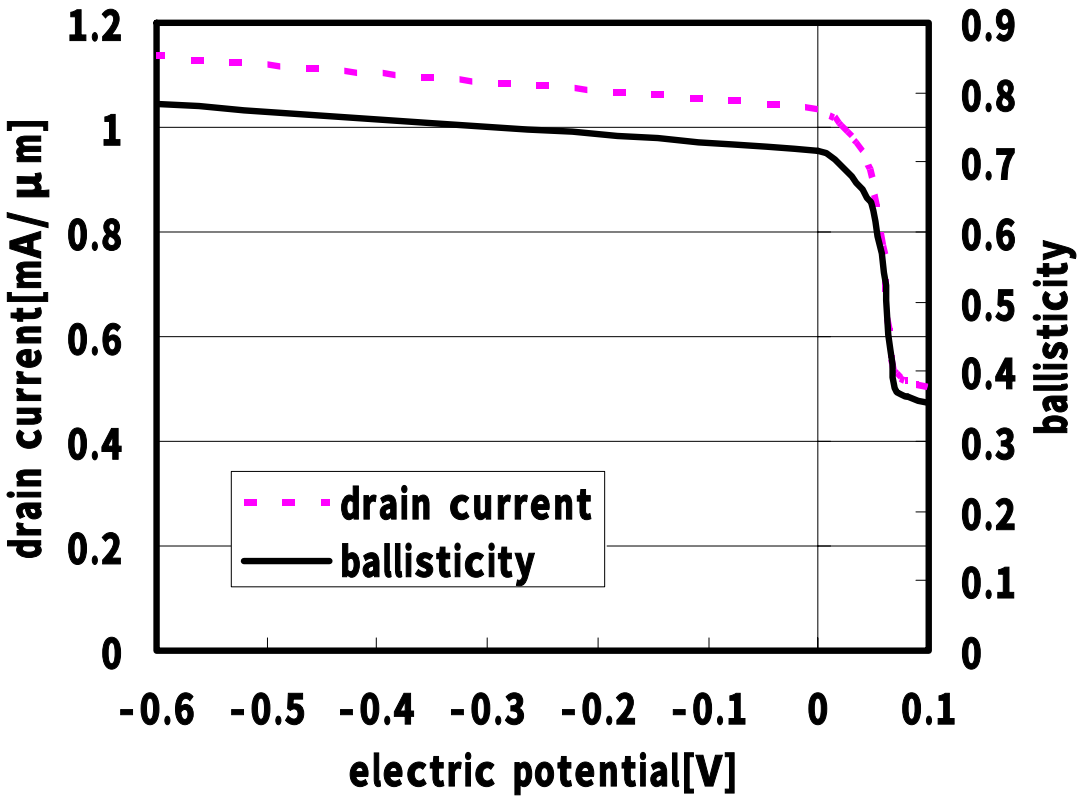

Figure 3.7 channel electric potential of the pattern 1 and ballistcity

To investigate the effects of channel electric potential to the ballisticity, we have calculated the ballisticity of a MOSFET with Lg=10[nm] and tox=0.5[nm] under the conditions of Vg=0.5[V], Vd=0.6[V], channel doping concentration =1x10^{18}[cm^{-3}] and drain doping concentration =1x10^{20}[cm^{-3}] by varying channel electric potential from 0.1 V to -0.6V as shown in Figure 3.6. Calculated results are shown in Figure 3.7. Calculated ballisticity and also the drain current changed drastically at around the channel potential of 0.06V. Since the energy of optical phonon emission in the silicon is 0.063[V], the drastic change at around the channel potential of 0.06V indicating that probability of the energy relaxation by the optical phonon emission drastically increases at around the channel potential of 0.06V.

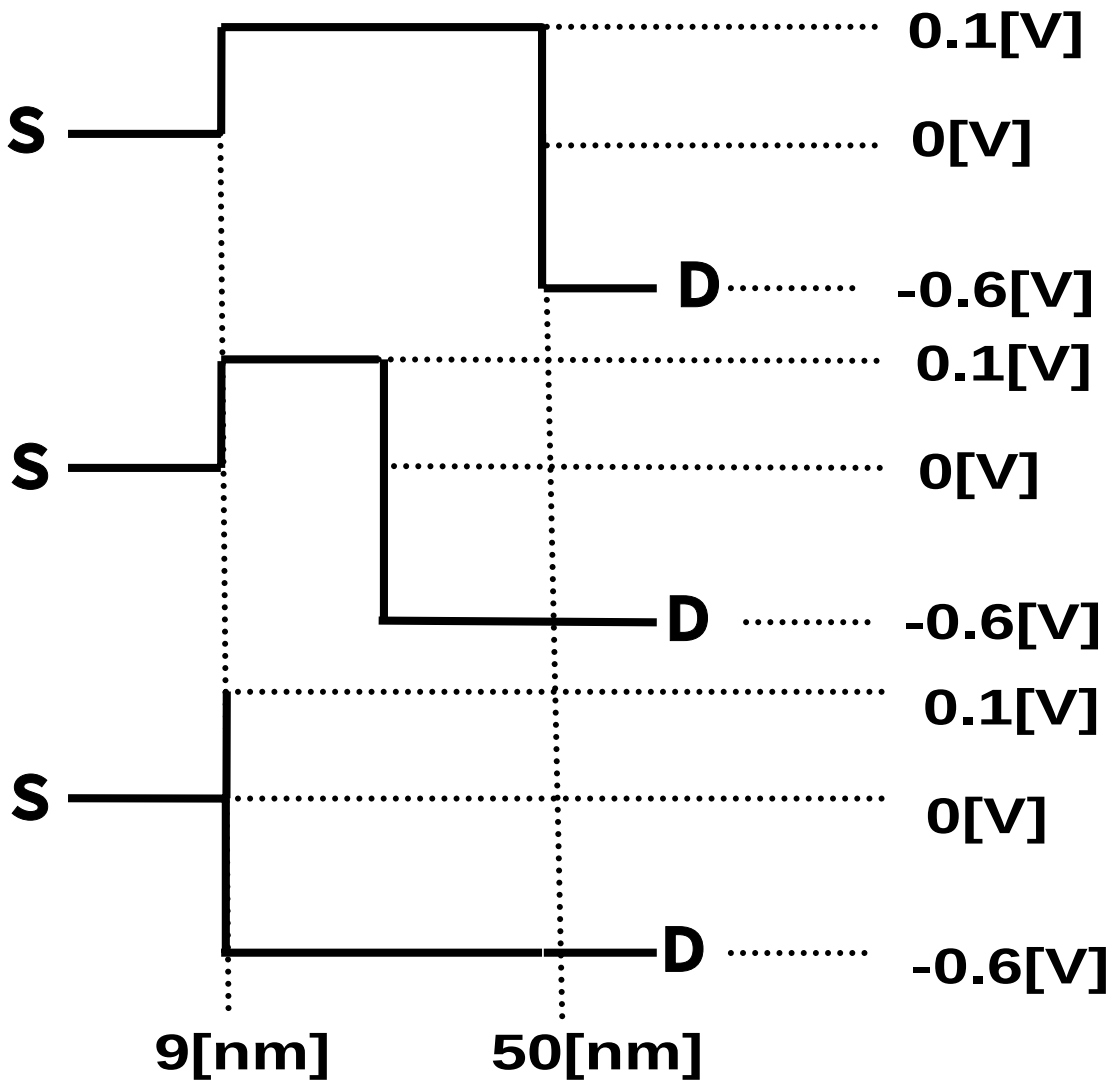

Figure 3.8 the pattern 2 of the position of channel electric potential behind the bottle neck

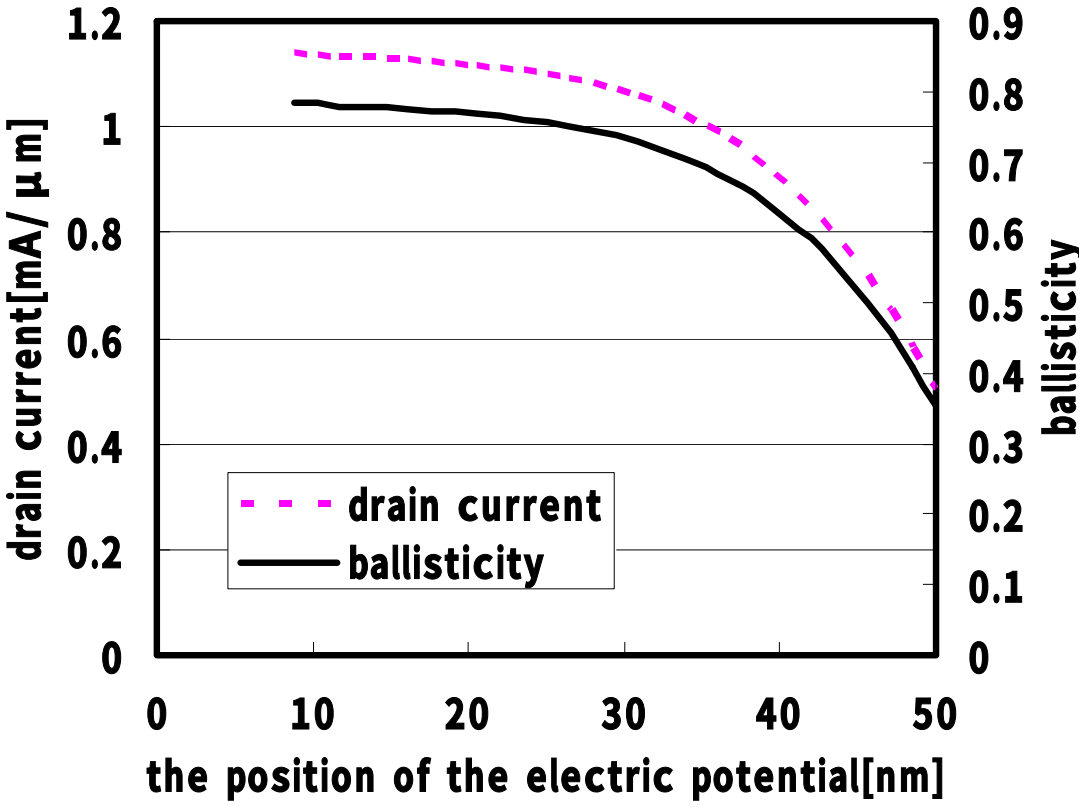

Figure 3.9 channel electric potential of the pattern 2 and ballistcity

we have calculated the ballisticity of a MOSFET with Lg=10[nm] and tox=0.5[nm] under the conditions of Vg=0.5[V], Vd=0.6[V], channel doping concentration =$1x10^{18}$[cm^{-3}] and drain doping concentration =$1x10^{20}$[cm^{-3}] by varying the position of channel electric potential from 9[nm] to 50[nm] as shown in Figure 3.8. Calculated results are shown in Figure 3.9. The ballisticity is changed in the drain side of the channel drastically. This phenomena show that there are many reflectional electros in the drain side of the channel than the source side of the channel. The ballisticity and the drain current is increase by the energy relaxation of these electrons.

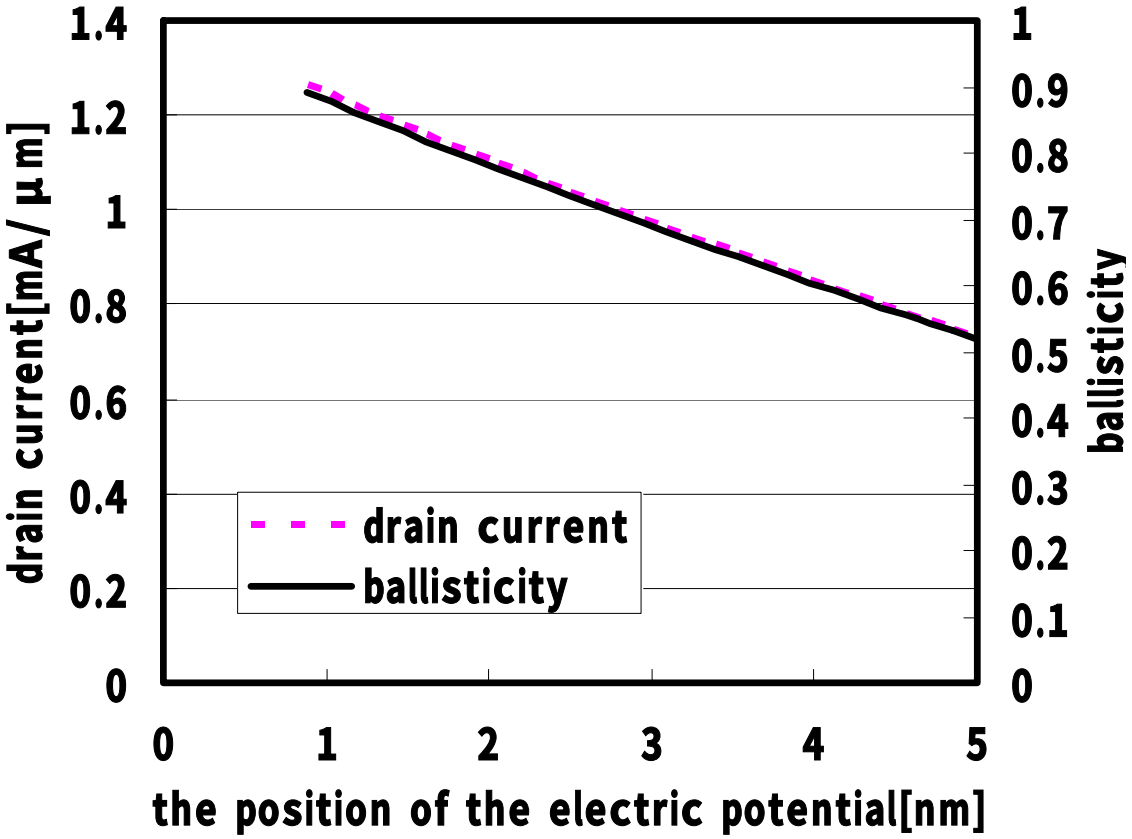

Figure 3.10 channel electric potential of the pattern 2 and ballistcity at the gate length 5[nm]

Figure 3.10 shows the position of the electric potential of figure3.8 in the gate length 5[nm]. Compared with figure 3.9, when the gate length is short, figure3.10 becomes the straight line. This shows that the ratio of reflectional electrons in the source side and the drain side are same.

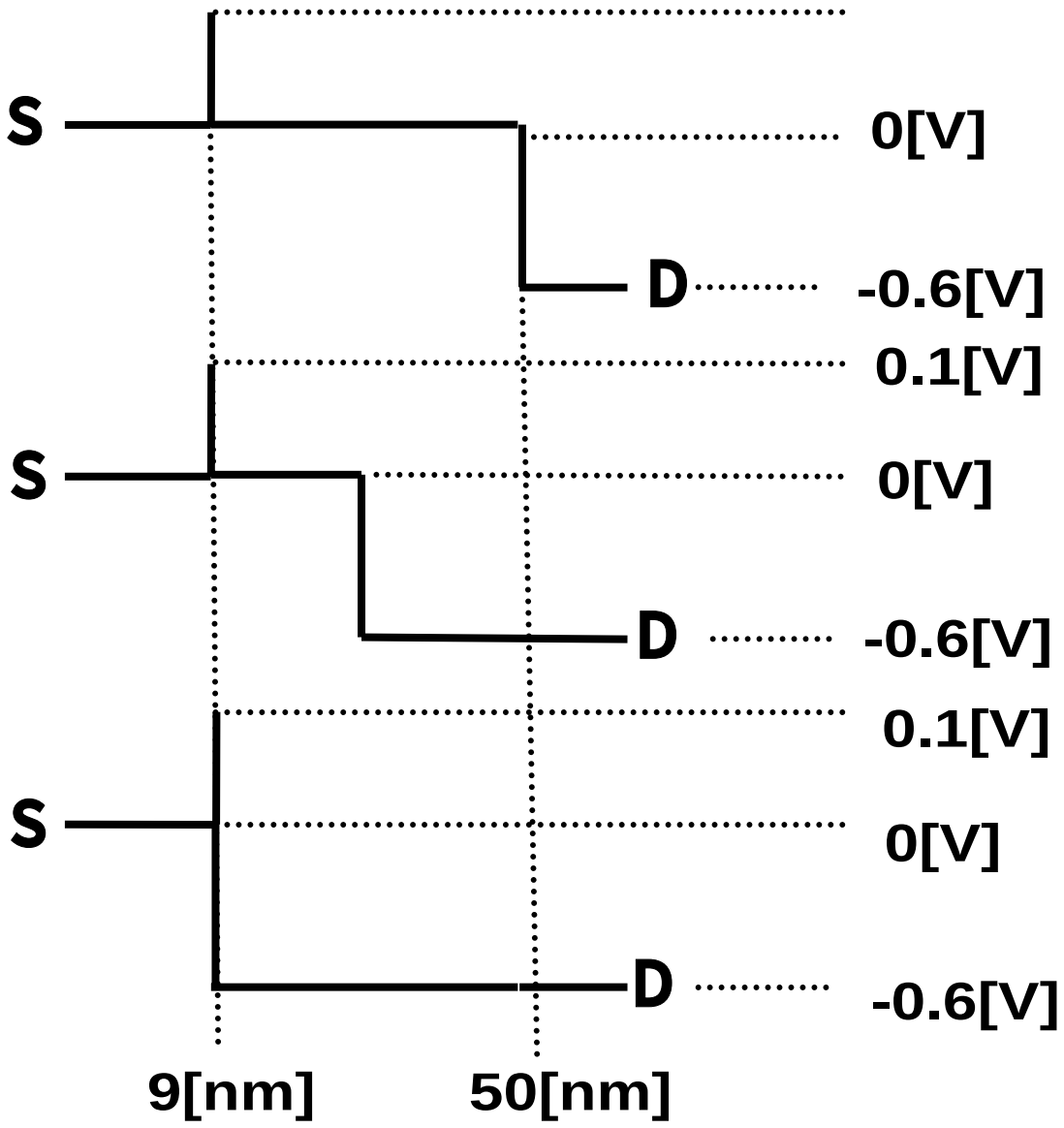

Figure 3.11 the pattern 3 of the position of channel electric potential behind the bottle neck

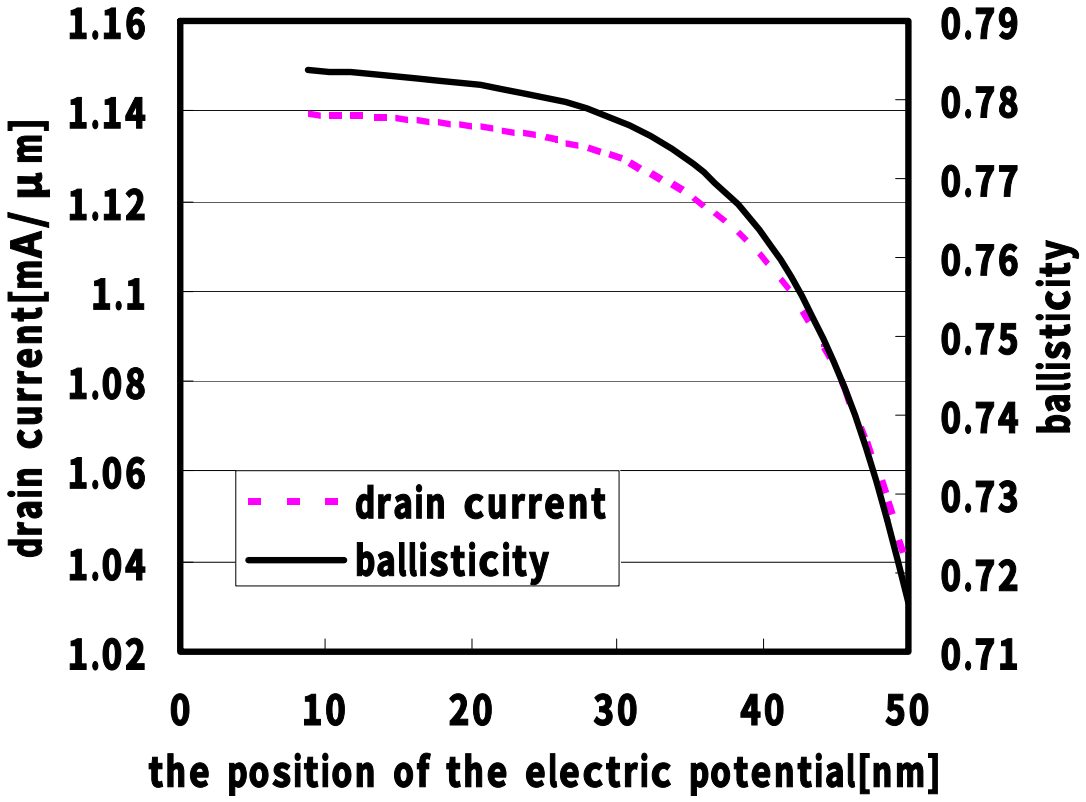

Figure 3.12 channel electric potential of the pattern 3 and ballistcity

we have calculated the ballisticity of a MOSFET with Lg=10[nm] and tox=0.5[nm] under the conditions of Vg=0.5[V], Vd=0.6[V], channel doping concentration =1x10^{18}[cm^{-3}] and drain doping concentration =1x10^{20}[cm^{-3}] by varying the position of channel electric potential from 9[nm] to 50[nm] as shown in Figure 3.11. Calculated results are shown in Figure 3.12. Compared with figure3.9, a change of ballisticity is small. This shows that the optical phonon is already effective.

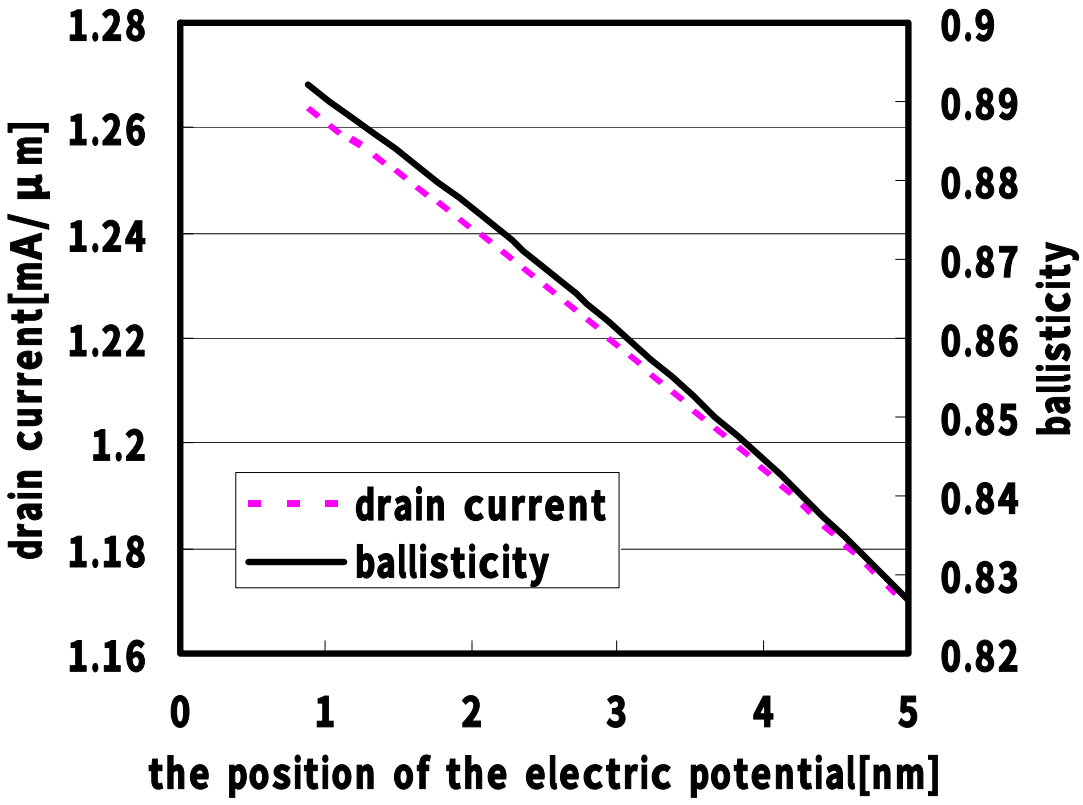

Figure 3.13 channel electric potential of the pattern 3 and ballistcity at the gate length 5[nm]

Figure 3.13 shows the position of the electric potential of figure3.11 in the gate length 5[nm]. Compared with figure 3.12, when the gate length is short, figure3.13 becomes the straight line by same reason about figure3.10. But a change of ballisticity is small because the optical phonon is already effective.

3.7 The operation of electric potential by doping

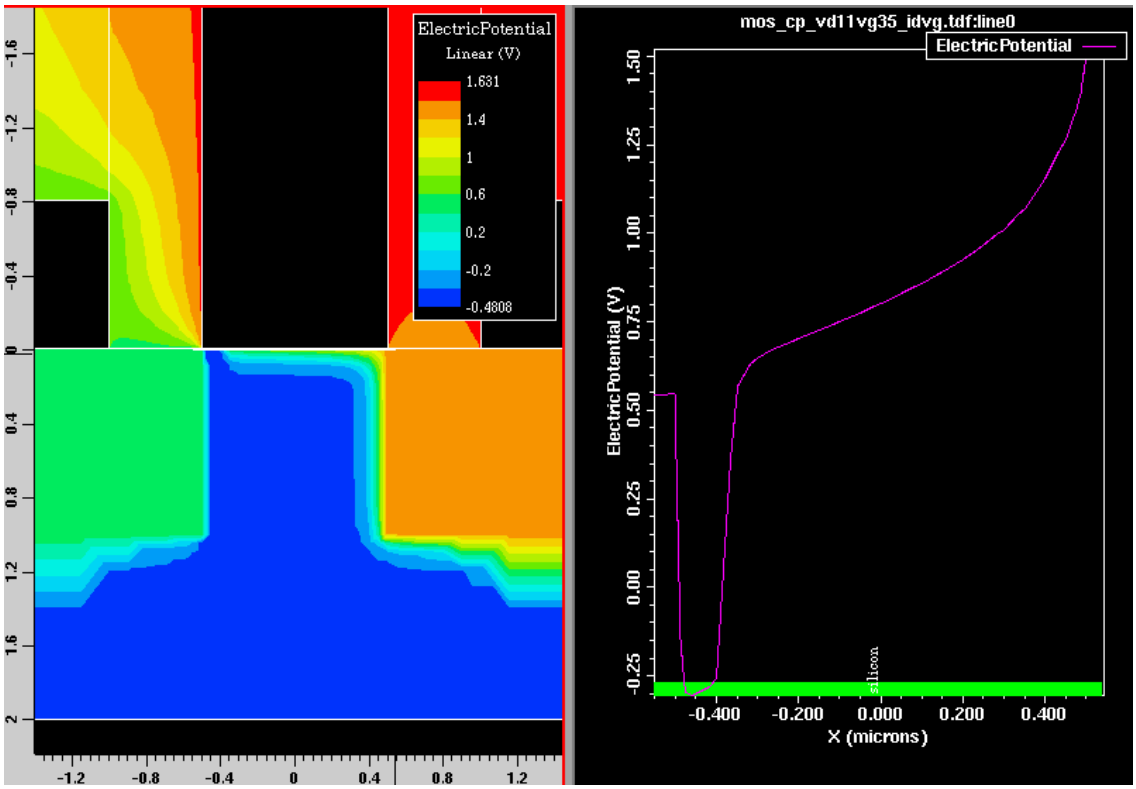

Figure 3.14 channel electric potential by the distribution of dope concentration in gate length 1 μ m

Figure 3.14 shows that Lg is 1μm, gate bias is 1[V], drain bias is 1[V], dope concentration of source・drain is $1\times10^{20}[cm^{-3}]$, dope concentration is $5\times10^{18}[cm^{-3}]$ at 100nm of the beginning of the channel, and dope concentration is $1\times10^{17}[cm^{-3}]$ at 900nm of the end of the channel.

The bottle neck is made at 100nm of the beginning of the channel and the channel potential falls at 900nm of the end of the channel. The drain current of this transistor increases than transistor of the normal dope concentration by chapter 3.6.

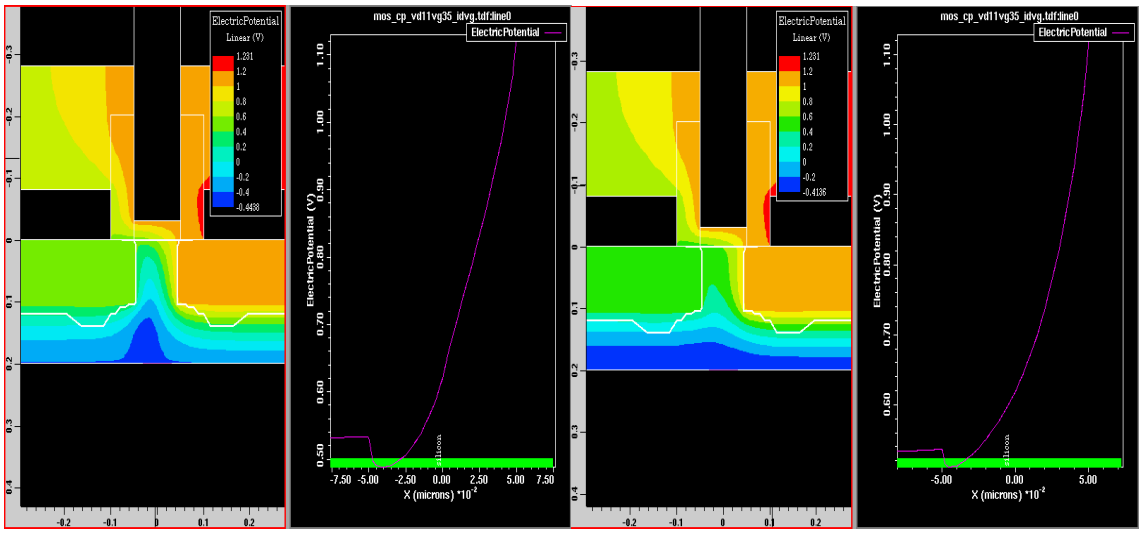

Figure 3.15 channel electric potential part 1 by the distribution of dope concentration in gate length 10nm

The left side of figure 3.15 shows that Lg is 10nm, gate bias is 1[V], drain bias is 1[V], dope concentration of source・drain is $1\times10^{20}[cm^{-3}]$, dope concentration is $5\times10^{17}[cm^{-3}]$ at the first half of the channel, and dope concentration is $1\times10^{17}[cm^{-3}]$ at the latter half of the channel. The right side of figure 3.15 shows dope concentration of the channel is $1\times10^{17}[cm^{-3}]$ and the other are the same value as the value of the left side of figure 3.15.

The size of the mountain of the electric potential in right and left figure is changing. But the drain current maybe does not change because quantity of change of the potential curve is few.

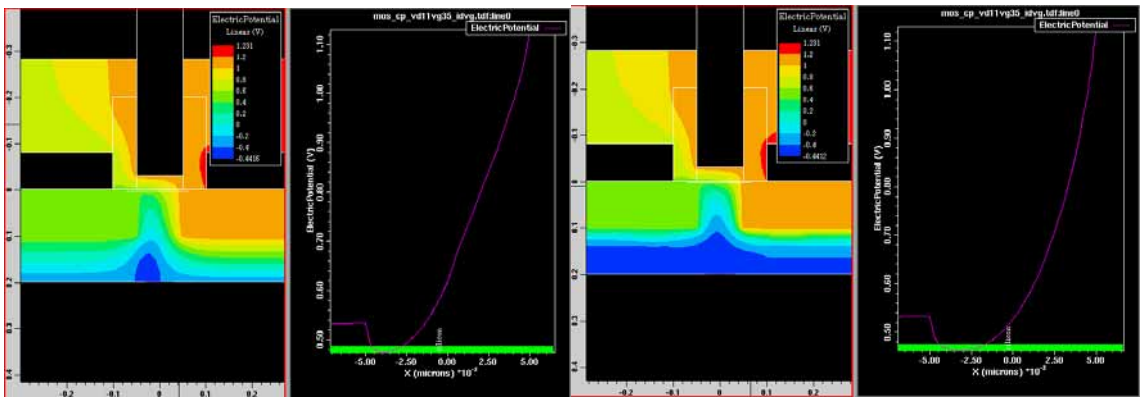

Figure 3.16 channel electric potential part 2 by the distribution of dope concentration in gate length 10nm

The left side figure of figure 3.16 shows that Lg is 10nm, gate bias is 1[V], drain bias is 1[V], dope concentration of source・drain is $1\times10^{20}[cm^{-3}]$, dope concentration is $5\times10^{17}[cm^{-3}]$ at the first half of the channel, and dope concentration is $1\times10^{16}[cm^{-3}]$ at the latter half of the channel. The right side figure of figure 3.16 shows dope concentration of the channel is $5\times10^{17}[cm^{-3}]$ and the other are the same value as the value of the left side of figure 3.16.

.

The length of the bottle neck of the electric potential in right and left figure is changing. But the drain current maybe does not change because quantity of change of the potential curve is few.

Chapter 4

Numerical analysis of three-dimensional transistor that uses High-k film

This chapter introduces research by Taurus and considers effect of DIBL by the dielectric constant distribution of the High-k film.

4.1.1 The present situation in the gate insulation film

The gate insulation film functions the capacitance of between the gate and channel, and this film need change the channel to the inversion layer which is the state to be filled with a carrier. The gate insulation film shrank by scaling, too. The one of the problems of the scaling of the gate insulation film is a leakage current on the insulation film. The leakage current is the tunnel current of the quantum mechanics effect by too short physical film length like figure 4.1. The existence of leakage current can not make the transistor function. Therefore the transistor need secure the physical film length not to be generated the tunnel current with having kept a function as the capacitance. This is high-k technology which adapts high dielectric constant materials to an insulation film. Even if a film thickness is big, high dielectric constant materials can function sufficiently as capacitance. Another problem by the scaling of the insulation film is the short channel effect. The line of electric force drops the electric potential of the channel because high dielectric constant film induces the line of electric force from the drain to the inside of the insulator film like figure 4.2. And figure4.3 shows that the line of electric force makes threshold voltage dropped.[4.1]

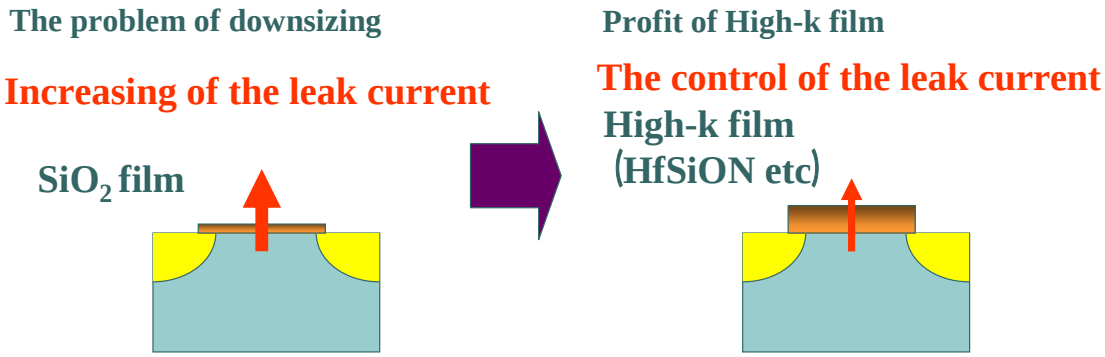

Year of Production	2005	2006	2007	2010	2013	2016
Physical Gate Length MPU (nm)	32	28	25	18	13	9
Equivalent physical oxide thickness for MPU Tox (nm)	0.8–1.3	0.7–1.2	0.6–1.1	0.5–0.8	0.4–0.6	0.4–0.5

Figure 4.1 high-k film and downsizing

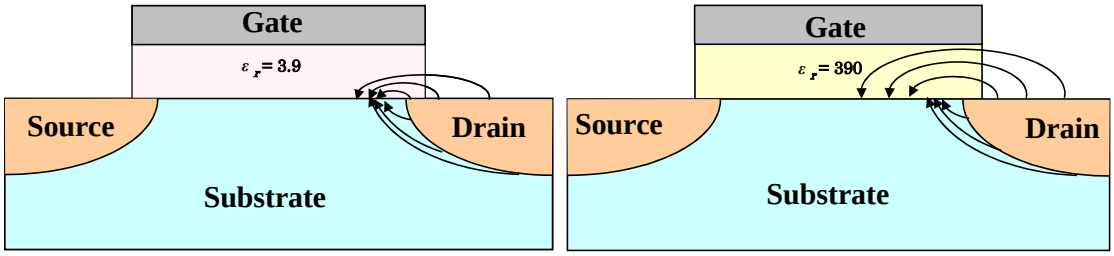

Figure 4.2 a high-k film and the line of electric force

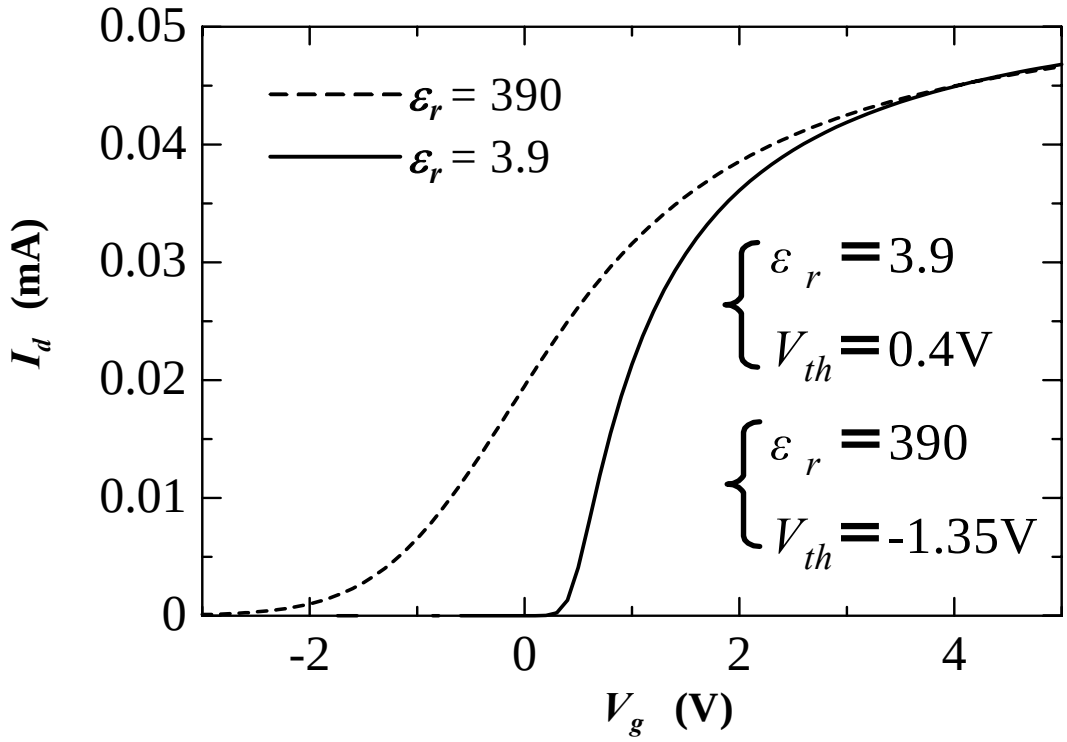

Figure 4.3 high-k film and threshold voltage

4.1.2 A research purpose and a supposition on the simulation

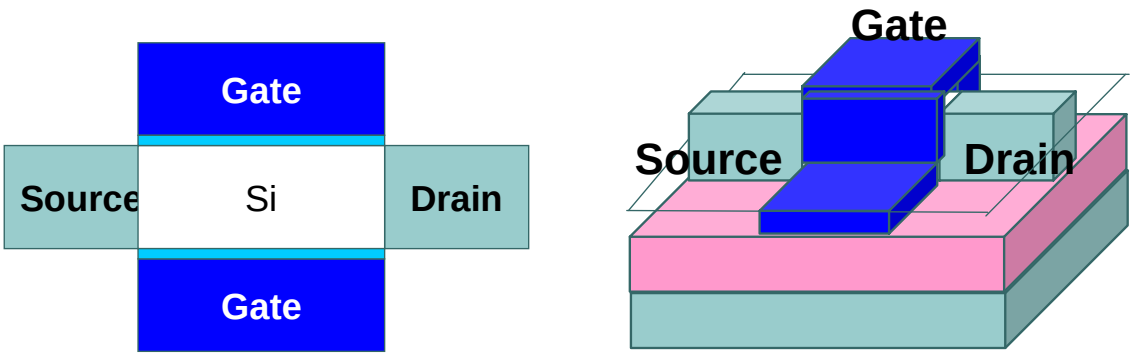

Figure 4.4 FinFET and its cross section

The left side of figure 4.4 is the cross section of the square line of right side of figure 4.4. This research estimates repression of the short channel effect by double gate structure FinFET which use high-k film.

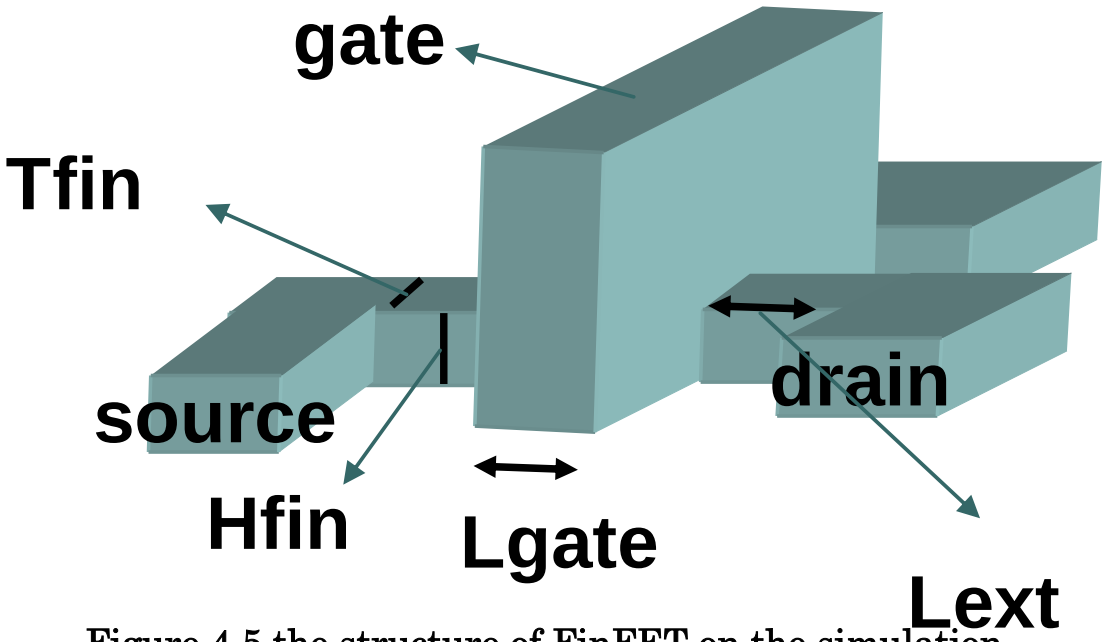

Figure 4.5 the structure of FinFET on the simulation

One of prerequisite on the simulation is Lgate=24[nm], Hfin=30[nm], Tfin=20[nm] EOT=1.2[nm] and no doping like channel in figure 4.5.

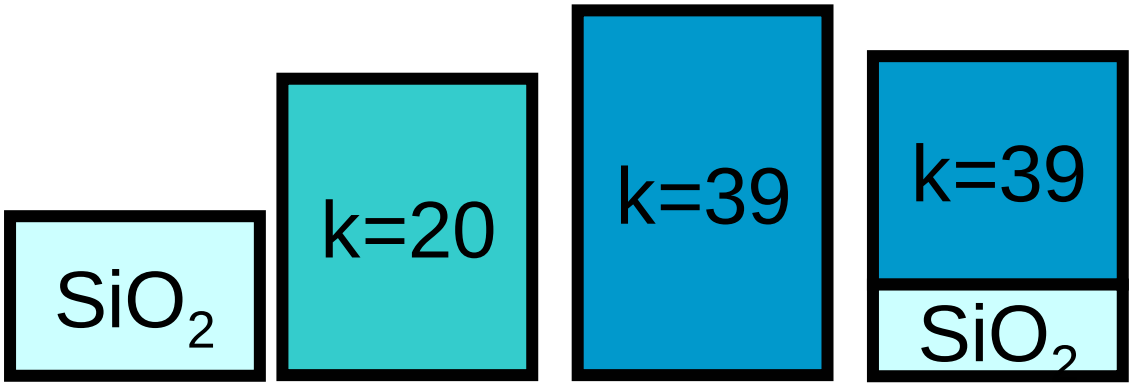

Figure 4.6 the dielectric constant of the insulation film on the simulation

Another of prerequisite on the simulation is a definition of SiO2(k=3.9) and virtual material（k=10, 20, 39）as an insulation film and a definition of laminating structure in figure 4.6. Here k is dielectric constant. And EOT of all structure of figure4.6 is the constant. The whole dielectric constant of laminating structure is 18.6.

4.2 An Id-Vg characteristic in changing a dielectric constant of Fin-FET

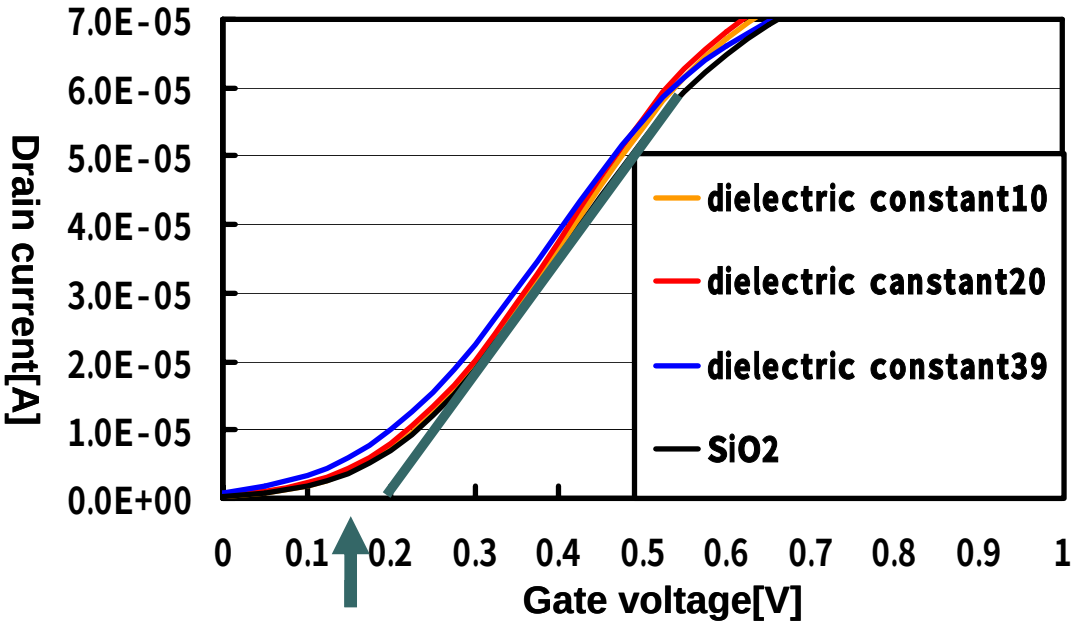

Figure 4.7 An Id-Vg characteristic in changing a dielectric constant of FinFET(Vd=0.1V)

Figure 4.7 is an Id-Vg characteristic in changing a dielectric constant of Fin-FET in Vd=0.1V. The threshold voltage becomes around 1.5[V] in all dielectric constant.

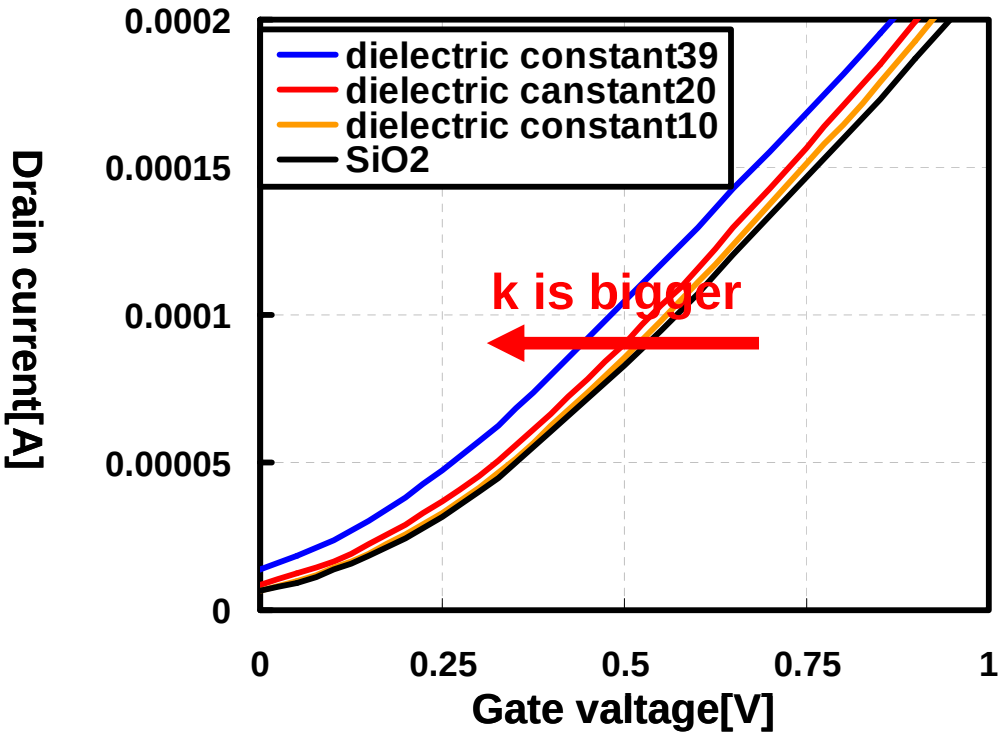

Figure 4.8 an Id-Vg characteristic in changing a dielectric constant of FinFET(Vd=1.0V)

Figure 4.8 is an Id-Vg characteristic in changing a dielectric constant of Fin-FET in This shows that high dielectric constant shifts the threshold voltage to the minus by short channel effect.

4.3 Comparison of the electric potential distribution in changing a dielectric constant of Fin-FET(k=39, 3.9)

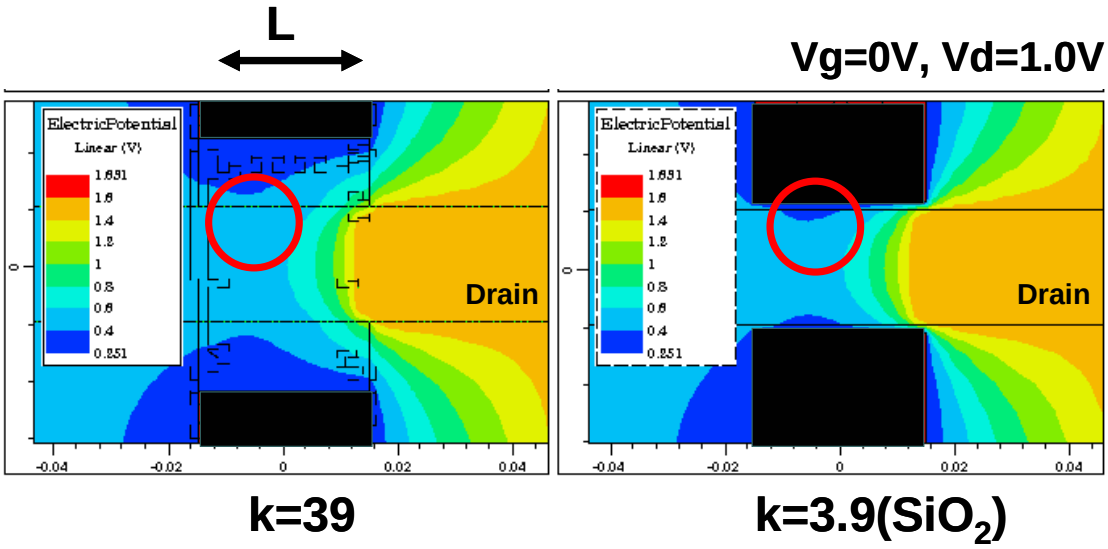

Figure 4.9 comparison of the distribution of the electric potential in changing a dielectric constant of Fin-FET(k=39, 3.9)

Figure 4.9 shows that the electric field of k=39 invades the circle of figure through the gate insulation film.

4.4 DIBL of each dielectric constant

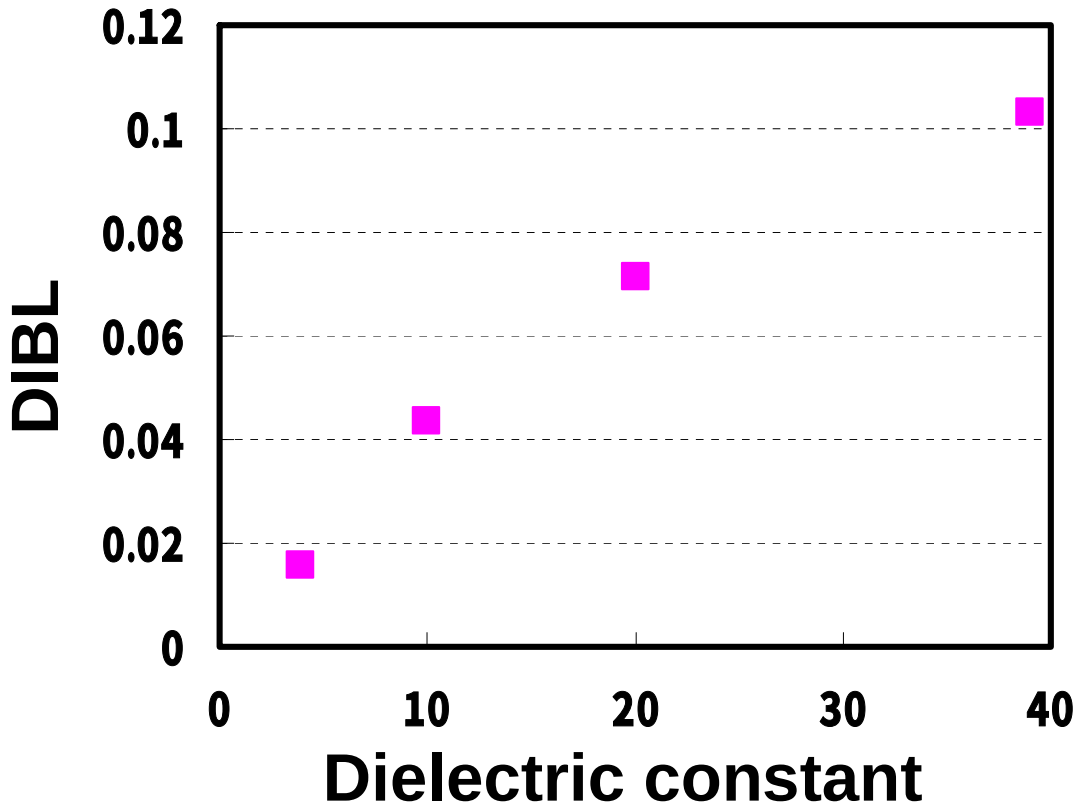

Figure 4.10 DIBL about each dielectric constant (k=39, 20, 10, 3.9)

Figure 4.10 show that DIBL is compared with Vd=0.1V and 1.0V. This shows that high dielectric constant promotes DIBL by the short channel effect.

4.5 A change of DIBL on the laminating structure

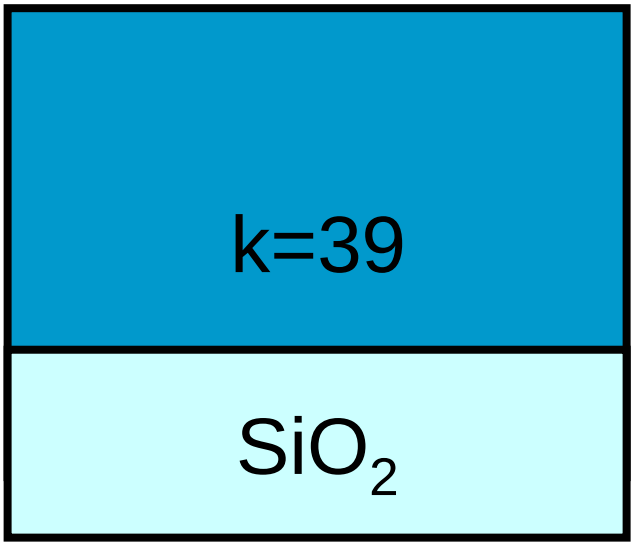

Figure 4.11 laminating structure of k=39 material and SiO2

Figure4.11 shows laminating structure of Sio2 and k=39 material. A reason to inspect the laminating structure is the existence of thin SiO2 of between Si and insulation films. SiO2 is made by thermodynamic reaction and SiO2 causes restraint of the deterioration of the mobility. Such a structure causes the incline of the dielectric constant in a film. So the influence of such a structure is inspected in the short channel effect.

At this time, DIBL is as follows.

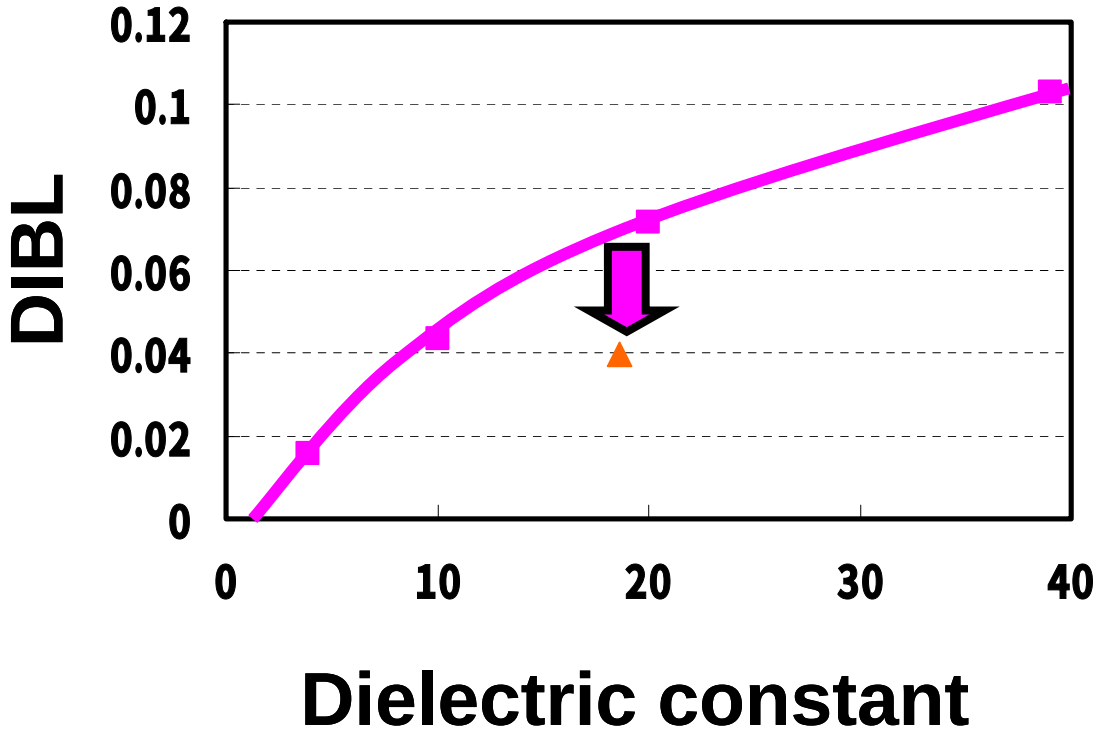

Figure 4.12 a change of DIBL by the dielectric constant of laminating structure

The triangular is DIBL of laminating structure in figure4.12. Figure4.12 shows that DIBL of laminating structure is less than DIBL of the material of dielectric constant 10. This shows that laminating structure is important about DIBL.

4.6 A change of electric potential by laminating structure

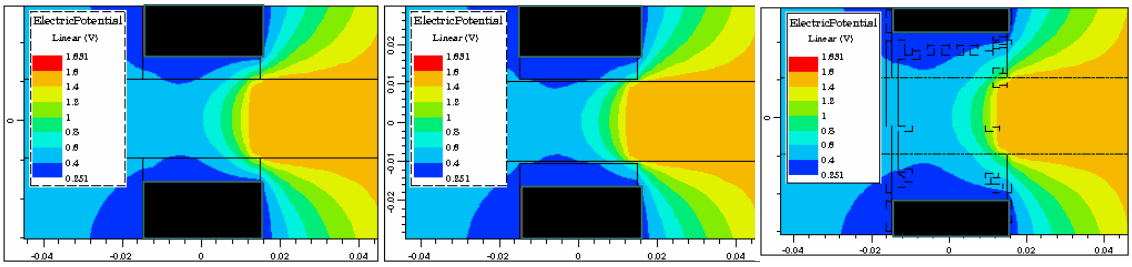

Figure 4.13 laminating structure and a change of electric potential

The left side of figure4.13 is electric potential of single layer of k=20. The central side of figure4.13 is electric potential of laminating structure of k=39 film and SiO2. The right side of figure4.13 is electric potential of single layer of k=39. Here Vg=0V, Vd=1.0V. This figure shows that laminating structure restrains the gate leakage current and short channel effect because SiO2 of laminating structure do not lead the line of the electric force to the whole channel.

4.7 Reference

[4.1] the master thesis of R.Fujiwara “Analysis on high-k dielectric gate insulator MISFETs by two-dimensional device simulation”, Mar.2001

Chapter 5

Conclusion

5.1.1 Conclusion of RT model

In summary, we have studied the preferred MOSFET structure for higher ballistic component in the drain current. Our studies on MOSFET structure with a gate length of 10[nm] show that the preferred conditions for obtaining higher ballistic current are the channel should be non-doped and the doping concentration in the drain should be less than $10^{20}[cm^{-3}]$. We also studied the effects of channel electric potential to the ballistic current.

5.1.2 Conclusion of Numerical analysis of three-dimensional transistor that uses High-k film

This research showed that high dielectric constant raises DIBL in constant EOT. This was the effect by the line of electric force through the insulation film.
And laminating structure of whole dielectric constant about 20 becomes low DIBL. This DIBL was less than the material of dielectric constant 10.

5.2 Consideration of the social significance

This research showed necessary structure for Ballistic conduction and if electric potential can be operated, the drain current and the ballisticity are increased. And this research showed that the control of the constant of the dielectric in an insulation film restrains a short channel effect.